



Research Article

Abu Hureyra, Syria, Part 1: Shock-fractured quartz grains support 12,800-year-old cosmic airburst at the Younger Dryas onset

Andrew M.T. Moore¹, James P. Kennett², Malcolm A. LeCompte³, Christopher R. Moore^{4,5}, Yong-Qing Li⁶, Gunther Kletetschka^{7,8}, Kurt Langworthy⁹, Joshua J. Razink⁹, Valerie Brogden⁹, Brian van Devener¹⁰, Jesus Paulo Perez¹⁰, Randy Polson¹⁰, Siddhartha Mitra¹¹, Wendy S. Wolbach¹² and Allen West^{13,*}

¹College of Liberal Arts, Rochester Institute of Technology, Rochester, NY 14623, USA; ²Department of Earth Science and Marine Science Institute, University of California Santa Barbara, Santa Barbara, CA 93106, USA; ³Elizabeth City State University, Center of Excellence in Remote Sensing Education and Research, Elizabeth City, NC 27909, USA; ⁴South Carolina Institute of Archaeology and Anthropology, University of South Carolina, Columbia, SC 29208, USA; ⁵SCDNR Heritage Trust Program, Land, Water, and Conservation Division, South Carolina Department of Natural Resources, Columbia, SC 27909, USA; ⁶Department of Physics, East Carolina University, Greenville, NC 27858, USA; ⁷Geophysical Institute, University of Alaska, Fairbanks, Alaska 99775, USA; ⁸Faculty of Science, Charles University, Albertov 6, Prague 12843, Czech Republic; ⁹CAMCOR, University of Oregon, 1443 E 13th Ave, Eugene, Oregon 97403, USA; ¹⁰Electron Microscopy and Surface Analysis Lab, Nanofab, University of Utah, Salt Lake City, UT 84112, USA; ¹¹Department of Geological Sciences, East Carolina University, Greenville, NC 27858, USA; ¹²Department of Chemistry and Biochemistry, DePaul University, Chicago, IL 60614, USA; ¹³Comet Research Group, 2204 Lakewood Drive, Prescott, AZ 86301, USA

*Correspondence to: Allen West, E-mail: CometResearchGroup@gmail.com, allen7633@aol.com

Received: 6 August 2023; Revised: 15 August 2023; Accepted: 23 August 2023; Published online: 28 September 2023

How to cite: Moore A.M.T., et al. Abu Hureyra, Syria, Part 1: Shock-fractured quartz grains support 12,800-year-old cosmic airburst at the Younger Dryas onset. *Airbursts and Cratering Impacts*. 2023 | Volume 1 | Issue 1 | Pages: 1–28 | DOI: 10.14293/ACI.2023.0003

ABSTRACT

A previous investigation revealed that shock-fracturing, a form of low-pressure shock metamorphism in quartz grains, can be produced during near-surface atomic airbursts and in cosmic impact structures, most likely at pressures lower than 8 GPa. This discovery implies that similar shock-fracturing may also form in quartz grains exposed to near-surface airbursts by comets and asteroids. Here, we investigate this hypothesis by examining quartz grains in a sedimentary profile from Abu Hureyra, a prehistoric archaeological site in northern Syria. This site was previously proposed to have experienced a nearby, low-altitude cosmic airburst at the onset of the Younger Dryas (~12,800 years ago). The Younger Dryas boundary layer (YDB) at Abu Hureyra has previously been shown to contain a rich assemblage of materials consistent in indicating a cosmic impact. These include anomalously high concentrations of melted micro-spherules displaying increased remanent magnetism; meltglass with low water content indicative of high-temperature melting; nanodiamonds, potentially including lonsdaleite; carbon spherules produced by biomass burning; black carbon or soot; total organic carbon; and abnormally high-temperature melted refractory minerals and elements, including platinum, iridium, chromite, and zircon. To further test this impact hypothesis, we searched for evidence of shocked quartz, a robust, widely accepted indicator of cosmic impacts. We used a comprehensive analytical suite of high-resolution techniques, including transmission electron microscopy (TEM) and electron backscatter diffraction (EBSD), to examine and characterize quartz grains from the YDB layer at Abu Hureyra. Our analyses revealed the presence of quartz grains with sub-planar, sub-parallel, and sub-micron-wide intragranular fractures, most likely produced by mechanical and thermal shock or the combination of both. Furthermore, these fractures are typically filled with amorphous silica (glass), a classic indicator of shock metamorphism. Elemental analyses of the weight percentages of oxygen in the amorphous silica indicate that this could not have formed from

the deposition of hydrated silica (e.g., opal and hyalite), which is enhanced in oxygen. Instead, the silica we observed is typically depleted in oxygen, consistent with melting under highly reducing conditions. The shock fractures in quartz grains also display Dauphiné twinning, which sometimes develops during the stress of high temperatures or pressures. This evidence is consistent with the hypothesis that the glass-filled fractures in quartz grains were produced by thermal and mechanical shock during a near-surface cosmic airburst at Abu Hureyra. These glass-filled fractures closely resemble those formed in near-surface atomic airbursts and crater-forming impact events.

KEYWORDS

cosmic airbursts, shocked quartz, shock fractures, scanning electron microscopy (SEM), electron backscatter diffraction (EBSD), transmission electron microscopy (TEM), cathodoluminescence (CL), Dauphiné twinning, nanodiamonds, iridium and platinum

Introduction

This article is the first of a three-part series about the archeological site at Abu Hureyra, Syria. Here, Part #1 concentrates on shock-fractured quartz as evidence of a local cosmic airburst; Part #2 [1] focuses on impact-related high-temperature meltglass, nanodiamonds, micro-spherules, iridium, and platinum; and Part #3 [2] proposes that multiple cosmic airbursts/impacts triggered Younger Dryas climate change that, in turn, initiated the transition from hunting-and-gathering to cultivation.

Shock metamorphism in quartz

In this study, “fractures” are defined as intragranular cracks in a quartz grain, characterized by wall displacement, and they are typically sub-parallel, sub-planar, and a few microns wide. In particular, we investigate whether the observed fractures formed by impact-related thermal or mechanical stress, commonly known as shock metamorphism, instead of by natural geologic processes. This study focuses primarily on the subset of shock fractures discontinuously filled with amorphous silica (a term we use interchangeably with “glass”), even though some shock fractures contain no detectable glass. However, it

is unclear whether these glass-filled features are actual fractures or, in some cases, are some other sub-planar amorphous silica discontinuities, perhaps low-pressure shock lamellae. In any event, amorphous silica is almost always associated with impact-related shock metamorphism.

Previous studies of cosmic impact structures have described shock fractures in quartz and given them various names, including shock extension fractures (SEFs) [3–6], shock fractures [7, 8], and vermicular (i.e., wormlike) microfractures [4, 6, 9]. Here, as in Hermes et al. [10] and previous studies, we adopt the term “shock fractures” to denote microfractures in quartz produced by thermal and mechanical shock.

Multiple studies have reported characteristics of the geologic and impact-related metamorphism types observed in quartz. These types include planar deformation features (PDFs) [11–22], planar fractures (PFs) [20, 23], tectonic deformation lamellae (DLs) [7, 13, 14, 16, 19, 20, 24–27], and sub-planar shock micro-fractures [22, 28–33]. Here, the term “lamellae” denotes closed high-pressure stress features in quartz, whereas “fracture” denotes lower-pressure shock features.

Table 1 compares some commonalities and differences among the types of metamorphic features in quartz [10]. Our analysis of previous work demonstrates that shock fractures

Table 1: Characteristics of metamorphism of quartz.

Characteristics	Shock fractures	PDFs	PFs	DLs
Fractures rather than lamellae	Yes	No	Yes	No
Features crystallographically controlled	No	Yes	Yes	Sometimes
Multiple oriented sets of fractures/lamellae	Weakly oriented	1–6+	1–6+	1–2
Planar fractures/lamellae	Sub-planar	Planar	Planar	Sub-planar
Parallel fractures/lamellae	Sub-parallel	Parallel	Parallel	Sub-parallel
Thickness of fractures/lamellae	nm to μm s	Usually $\leq 1 \mu\text{m}$	Usually $\geq 3 \mu\text{m}$	Usually $\geq 2 \mu\text{m}$
Features filled with amorphous silica	Often	Often	Sometimes	Never
Spacing between fractures/lamellae	nm to μm s	Usually $< 1 \mu\text{m}$	Usually $> 20 \mu\text{m}$	Usually $\geq 5 \mu\text{m}$
Estimated formation pressure (Gpa)	≥ 3	$\sim 10\text{--}25$	< 10	< 1
Estimated formation speed	$< 1 \text{ sec}$	$< 1 \text{ sec}$	$< 1 \text{ sec}$	Very slow
	Shared features:	2 of 10	4 of 10	2 of 10

Previous studies of shock fractures [4, 8, 28, 29, 34] share 2 of 10 characteristics with planar deformation features (PDFs), 4 of 10 characteristics with planar fractures (PFs), and 2 of 10 with tectonic deformation lamellae (DLs). The green shading represents features in common with shock fractures in our study. Data are primarily derived from French and Koeberl [20]. The table is adapted from Hermes et al. [10] and is used under Creative Commons, CC by 4.0 (<http://creativecommons.org/licenses/by/4.0/>).

are significantly different from PDFs, PFs, and DLs. The most critical reported differences are that shock fractures are typically sub-planar rather than planar, sub-parallel rather than parallel, not crystallographically oriented, and form at lower shock pressures (see Table 1).

Abu Hureyra and the Younger Dryas impact hypothesis

This contribution presents new, comprehensive evidence of shock-fracturing of quartz grains supporting the hypothesis that a near-surface cosmic airburst occurred ~12,800 years ago over northern Syria and destroyed the well-known prehistoric village of Abu Hureyra (AH) [35–37]. Archeological investigations at this site (Figure 1) by Moore et al. [1, 36–38] revealed that the site was continuously occupied by humans who initially practiced hunting-and-gathering in the late Epipaleolithic (~13,400 cal BP) before transitioning to

full-scale farming by the early Neolithic (~7,500 cal BP) [1]. Moore et al. [2] proposed that the Younger Dryas (YD) impact event (~12,800 cal BP) abruptly triggered YD climate change, which produced cooler, drier conditions at Abu Hureyra. These changes, in turn, caused the villagers to begin practicing the earliest known continuous cultivation of domestic-type grains and legumes and to start tending livestock [39], fundamental steps that eventually developed into full-scale agriculture and animal husbandry over subsequent millennia.

This impact event at Abu Hureyra is an integral part of the Younger Dryas Impact Hypothesis that posits multi-continental cosmic airbursts/impacts recognized at >50 locations spanning >100 million km² across North and South America, Europe, Asia, and Africa [35, 40–64]. Here, “airburst” refers to a near-surface atmospheric detonation by a cosmic object, resulting in a high-temperature, hypervelocity

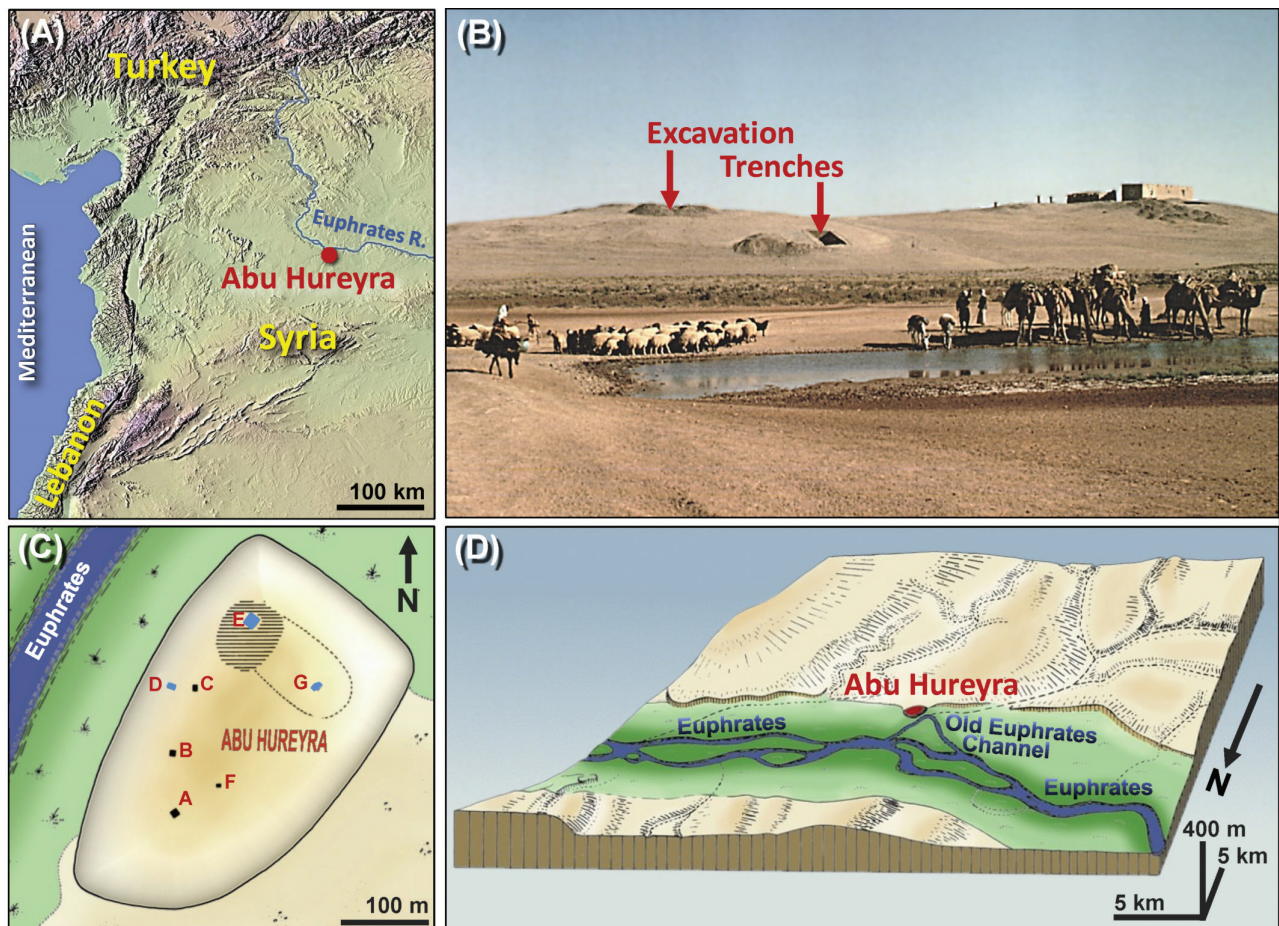


Figure 1: Location of Abu Hureyra. (A) Map of the Middle East, showing Abu Hureyra’s location along the Euphrates River in Syria. (B) Photograph of the large Abu Hureyra tell shows the locations of several key excavation trenches. (C) Map of the Abu Hureyra tell, showing locations of excavation trenches labeled A through G. Sediment samples from Trenches D, E, and G (small blue rectangles) contain the YDB layer, identified by peak abundances of impact-related proxies, including nanodiamonds, micro-spherules, meltglass, and platinum. (D) Artist’s depiction of the Abu Hureyra site at the YD onset (~12,800 cal BP), located along the floodplain edge close to a now-abandoned braid of the Euphrates River. Adapted from Moore et al. [1, 37, 38], usable under Creative Commons, CC by 4.0 (<http://creativecommons.org/licenses/by/4.0/>).

jet of ionized gases and debris that reaches Earth's surface [65–67].

The Younger Dryas was a significant climatic event between 12.8 ka and 11.6 ka that broadly triggered cooling in the North Hemisphere at high- to mid-latitudes and warming in high- to mid-latitudes of the Southern Hemisphere [54]. The impact layer has been named the YD boundary layer or YDB, a term used here to signify the YD onset ~12,800 years ago [49] rather than its termination [40].

Study objective

It is well established that shocked quartz characteristics can be formed and represent a proxy of cosmic impact events. However, most previous shocked quartz studies focused on its formation under extremely high pressures and temperatures produced by large, crater-forming impact events [10]. In contrast, few investigations have examined quartz shock features that may form at lower pressures and temperatures produced by non-crater-forming airbursts and impacts that form small craters. Since smaller airbursts and impacts have occurred more commonly in the past than large crater-forming events [65, 67], it is crucial that shocked quartz be comprehensively studied to recognize these smaller events in the geologic record. Hence, this study of shocked quartz was stimulated by the observations of Hermes et al. [10], who investigated shock-fractured quartz grains from Arizona's Meteor Crater, a 1.2-km-wide impact structure, and compared the grains to those from the 1945 near-surface Trinity nuclear airburst at the Alamogordo Bombing Range, New Mexico, and two airbursts at a Kazakhstan test site in 1949 and 1953. This investigation demonstrated that glass-filled shock fractures and Dauphiné twinning in quartz could form during near-surface nuclear airbursts and crater-forming impact events in which the high-temperature, high-pressure fireball is coupled with Earth's surface. This discovery implied that these features may also form during near-surface cosmic airbursts.

Our study investigated thin-sectioned individual quartz grains from the Abu Hureyra sequence in search of similar glass-filled shock fractures and Dauphiné twinning. We tested the hypothesis that if the previously identified cosmic impact proxies indicate a high-energy near-surface airburst near Abu Hureyra, as previously posited, this impact may also have produced shock metamorphism in quartz grains preserved in the YDB cosmic impact layer but not in adjacent sediments above and below.

Previous reports of YDB shocked quartz

Although no shock metamorphism of quartz grains has previously been identified from the Abu Hureyra site, potentially shocked quartz grains have been reported in YDB-age sediments in four other sites: Demitroff et al. [68] from Newtonville, New Jersey (12,783 ± 29 cal BP); Mahaney [46] from the MUM 7B site in the Venezuelan Andes (12,787 ± 30 cal BP); Ballard and Bijkerk [69] near Ossendrecht,

Netherlands (~12,870–13,200 cal BP); and Van Hoesel et al. [70] a single classically shocked quartz grain at Aalsterhut, Netherlands (12,740–12,710 cal BP). Other than Van Hoesel et al. [70], these studies were limited in scope for the analytical techniques employed for the robust characterization of shocked quartz. In the case of the study by Van Hoesel [70], only one shocked quartz grain was found and described, and the presence of this grain was attributed to reworking (secondary deposition) into sediments of YDB age. Nevertheless, these investigations, along with the results of Hermes et al. [10] for the nuclear airbursts, encouraged us to search for shocked quartz at Abu Hureyra. We chose this site because of its importance as an archeological site, the presence of the YDB cosmic impact layer, and robust radiocarbon dating.

Site setting stratigraphy and chronology

Abu Hureyra is an ancient settlement mound or “tell” in northern Syria adjacent to the Euphrates River floodplain [1, 38] (Figure 1). The site is situated on the southwest bank of a bend in the Euphrates River atop a low terrace that was above the flood level of the river valley (Figure 1D). A dam across the river was completed in 1974; today, the site is submerged beneath the surface of the reservoir, precluding further above-water access.

In 1972 and 1973, several trenches were excavated through anthropogenically-deposited sandy Quaternary alluvium to bedrock, which consists predominantly of chalky limestone intercalated with thin beds of fine-grained chert and marls of Middle and Upper Eocene age [38]. Trench E was ~122 m from Trench D and ~110 m from Trench G; Trenches D and G are ~175 m apart [38] (Figure 1C). All the trenches contain archaeological strata deposited over bedrock [38].

Immediately above bedrock in Trench E, Moore et al. [38] identified a bed of unconsolidated, brown, limey sand (thickness: ~10 to 50 cm) of Allerød age (range: ~13,380 to 12,800 cal BP). Just above the Allerød bed, they also identified an ~12,800-year-old layer, a thin bed of unconsolidated, dark-brown, charcoal-rich sand with a thickness of ~3 to 5 cm at ~405 cm below surface (cmbs) [38], which is the YDB layer. The YDB stratum was overlain by a gray limey sand layer that varied in thickness from ~15 to 60 cm and ranged in age from ~12,800 to 11,700 cal BP [37, 38], spanning the Younger Dryas climate episode. This bed, in turn, was overlain by several meters of Holocene-age limey clay derived from the erosion of successive mudbrick buildings that extend to the ground surface [38]. We adopted the Bayesian-modeled calibrated radiocarbon age of 12,800 ± 40 cal BP at 68% CI for the YDB layer as used in Moore et al. [1].

Methods

At Abu Hureyra, eight available sediment samples that discontinuously span the YDB layer were investigated for candidate grains of shocked quartz (Table 2). A single 26 ×

Table 2: Stratigraphic distribution by depth of potential cosmic impact-related indicators and other proxies for the Abu Hureyra sequence.

Level #	Sample #	Depth (cm)	Shocked Quartz	Nanodiamonds (ppb)	Magnetic spherules (#/kg)	Meltglass (g/kg)	Plant-imprinted glass	Organic material (mL/L)	Carbon spherules (#/kg)	Soot (%)
19	ES4	82	No	0	0	0.00	Yes	–	15	–
337	ES7	192	No	0	0	0.00	Yes	–	0	–
361	ES10	202	No	0	0	0.02	Yes	–	0	–
362	ES11	222	No	0	0	0.04	Yes	–	0	–
402–406	ES14	350	No	0	0	0.23	Yes	–	0	0.28
445	E301	405	Yes	443	595	15.76	Yes	245.0	152	6.40
435	ES15	432	No	0	20	0.66	Yes	–	0	0.24
470	E326	446	No	–	0	tr	Yes	0.25	–	–

Glass-filled, shock-fractured quartz results are from this study; other proxies are from previous investigations [1, 2, 35, 37, 58].

46-mm thin-sectioned slide was prepared and analyzed for each sample (see Appendix, Methods). We employed a comprehensive suite of analytical techniques and instruments to study these thin sections. These included optical transmission microscopy (OPT), epi-illumination microscopy (EPI), scanning electron microscopy (SEM), energy dispersive spectroscopy (EDS), focused ion beam milling (FIB); transmission electron microscopy (TEM); scanning transmission electron microscopy (STEM); fast-Fourier transform (FFT); electron backscatter diffraction (EBSD); cathodoluminescence (CL); and micro-Raman. All procedures and instruments are discussed in detail in Appendix, Methods below. Each slide was carefully searched for candidate grains of shocked quartz using optical and transmission microscopy. Grains exhibiting closely-spaced, oriented fractures are considered candidates for shocked quartz, with each requiring focused investigations using multiple techniques. Descriptions of techniques presented below are adapted from Hermes et al. [10], which shares ten co-authors with the current study. These descriptions are publishable under Creative Commons, CC by 4.0 (<http://creativecommons.org/licenses/by/4.0/>).

Results and interpretations using multiple techniques

We observed no candidates for shock-fractured quartz in all samples above and below the YDB layer (E301) at 405 cm (Table 2), which was previously identified through the presence of multiple cosmic impact-related proxies. For this sample (E301), ~700 quartz grains were analyzed at a concentration of ~837 grains/cm². We found no classic high-pressure shock lamellae (PDFs and PFs), but of the quartz grains examined, 24 displayed potential low-shock fractures, all of which contained amorphous silica. Some features may have been shock lamellae, but we could not distinguish the difference. Four were confirmed using multiple techniques as shock-fractured quartz grains for a

ratio of ~1 per 175 grains. The other 20 grains are excellent candidates for shock-fractured quartz but were not exhaustively investigated and identified using all available techniques.

The identification of glass-filled, shock-fractured quartz requires multiple observations collectively using numerous analytical approaches. By necessity, therefore, the results of this investigation are graphic-intensive and presented in this contribution as multiple images and descriptive captions for each of the analytical techniques.

Epi-illumination microscopy (EPI) [10]

This analytical technique of reflected-light optical microscopy is valuable in viewing HF-etched quartz grains (Figure 2) displaying glass-filled fractures. Multiple studies have demonstrated the importance of performing such analyses after etching quartz grains with HF [7, 13, 14, 16, 71, 72]. According to Gratz et al. [14], the HF-etching removes some amorphous silica that filled the shock features, allowing for the “*unambiguous visual distinction between glass-filled PDFs and glass-free tectonic deformation arrays in quartz.*” Nevertheless, other techniques are still necessary to identify and characterize the filled material as amorphous silica, a key indicator of shock metamorphism [13, 14].

In contrast, tectonic stress lamellae are not visible in EPI as open fractures in geologically-deformed grains but may appear as shallow, closed depressions that lack filling amorphous silica. We tested this by examining six tectonically-deformed quartz grains and six unshocked natural quartz grains, revealing that none contain amorphous silica. All grains are from Abu Hureyra sample E301.

Optical transmission microscopy (OPT) [10]

Representative optical images of quartz grains are shown in Figure 2. Most display a single set of shock fractures, meaning all are oriented in approximately the same direction. However, a few grains display multiple sets or multiple non-oriented individual fractures.

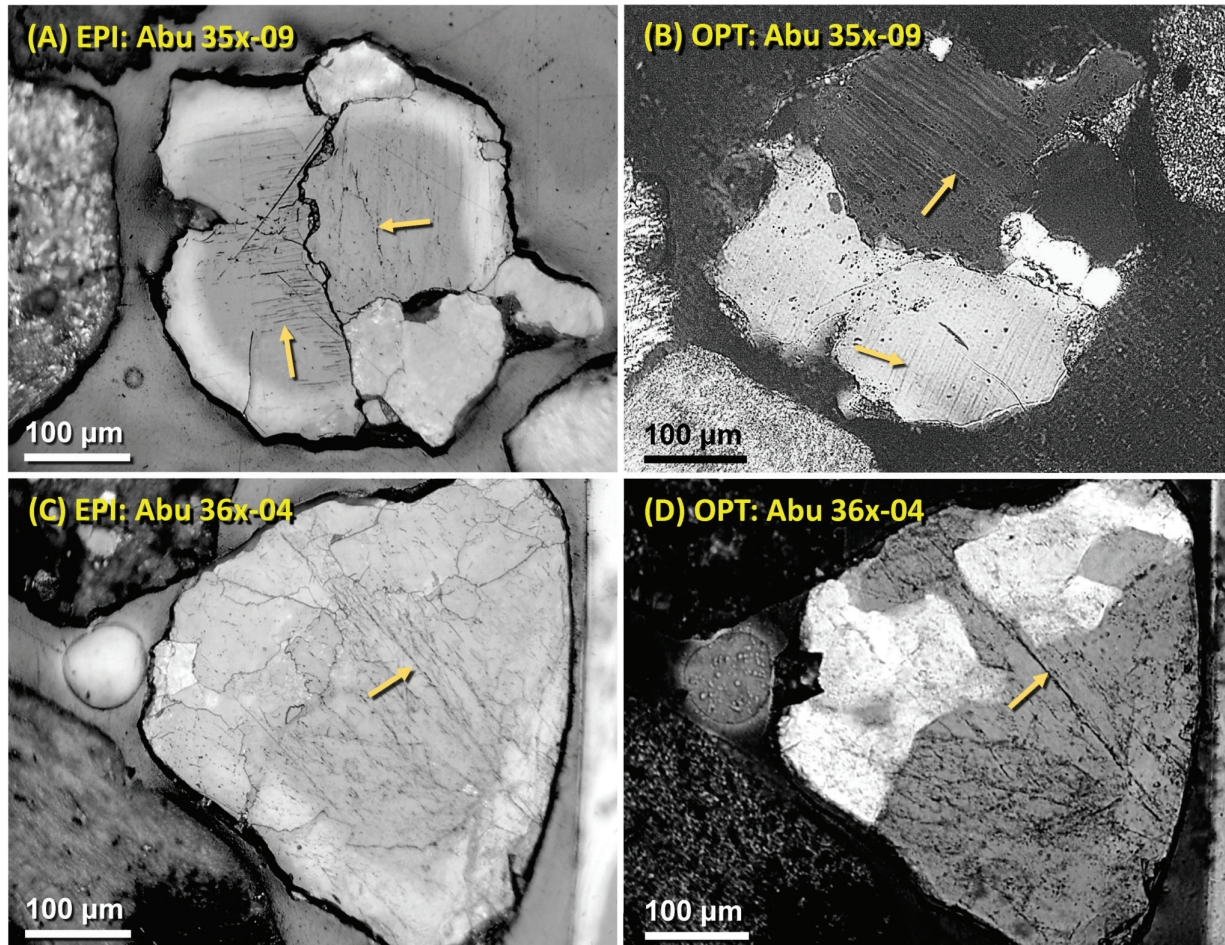


Figure 2: Epi-illuminated microscopy (EPI) and optical transmission microscopy (OPT), images of shock-fractured quartz grains. (A-B) ~460-µm-wide polycrystalline quartz grain 35x-09. (C-D) ~465-µm-wide polycrystalline quartz grain 36x-04. Gold arrows in epi-illumination (EPI) images (left column) indicate randomly selected shock fractures. The fractures were not easily visible with optical microscopy or epi-illumination before HF-etching. Optical images (right column) were acquired under crossed polarizers with dark-to-light contrasting areas, indicating the polycrystalline nature of the grains. Images were acquired with polarizers rotated $\sim 10^\circ$ off maximum for better visibility.

Scanning electron microscopy (SEM) [10]

SEM backscatter secondary electron (BSE) analyses revealed filled fractures in quartz grains that appear mostly as sub-linear features, although some are curvilinear (Figures 3 and 4). Additional analyses were also necessary to identify and characterize the material filling the fractures.

Scanning transmission electron microscopy (STEM) [10]

FIB locations on the grains analyzed are shown in Figures 3 and 4. Using bright-field STEM, the 8- to 15-µm-wide foils display inter-fracture spacings ranging from ~ 250 nm to 3 µm. Nearly all shock fractures were observed to contain material that other analyses show to be amorphous silica. In contrast, HF-etched grains with visible tectonic deformation lamellae have not been observed to display any associated

amorphous silica [10]. Similarly, unshocked, HF-etched, natural quartz grains display no visible lamellae [10].

Cathodoluminescence (CL) [10]

Representative CL images are shown in Figures 3 and 4. Under CL, fractures filled with amorphous silica have been reported to be commonly non-luminescent, i.e., black [16, 73, 75]. However, some amorphous silica has been reported to luminesce as red [76]. Alternately, natural, open fractures also appear black, and therefore, the possible presence of amorphous silica must be confirmed using TEM. Some sub-planar structures luminesce black and are not associated with fractures, thus indicating amorphous silica. According to previous studies [16, 73–75], if quartz luminesces red, it usually has been heated or melted and then recrystallized but no longer contains amorphous silica. Tectonic deformation

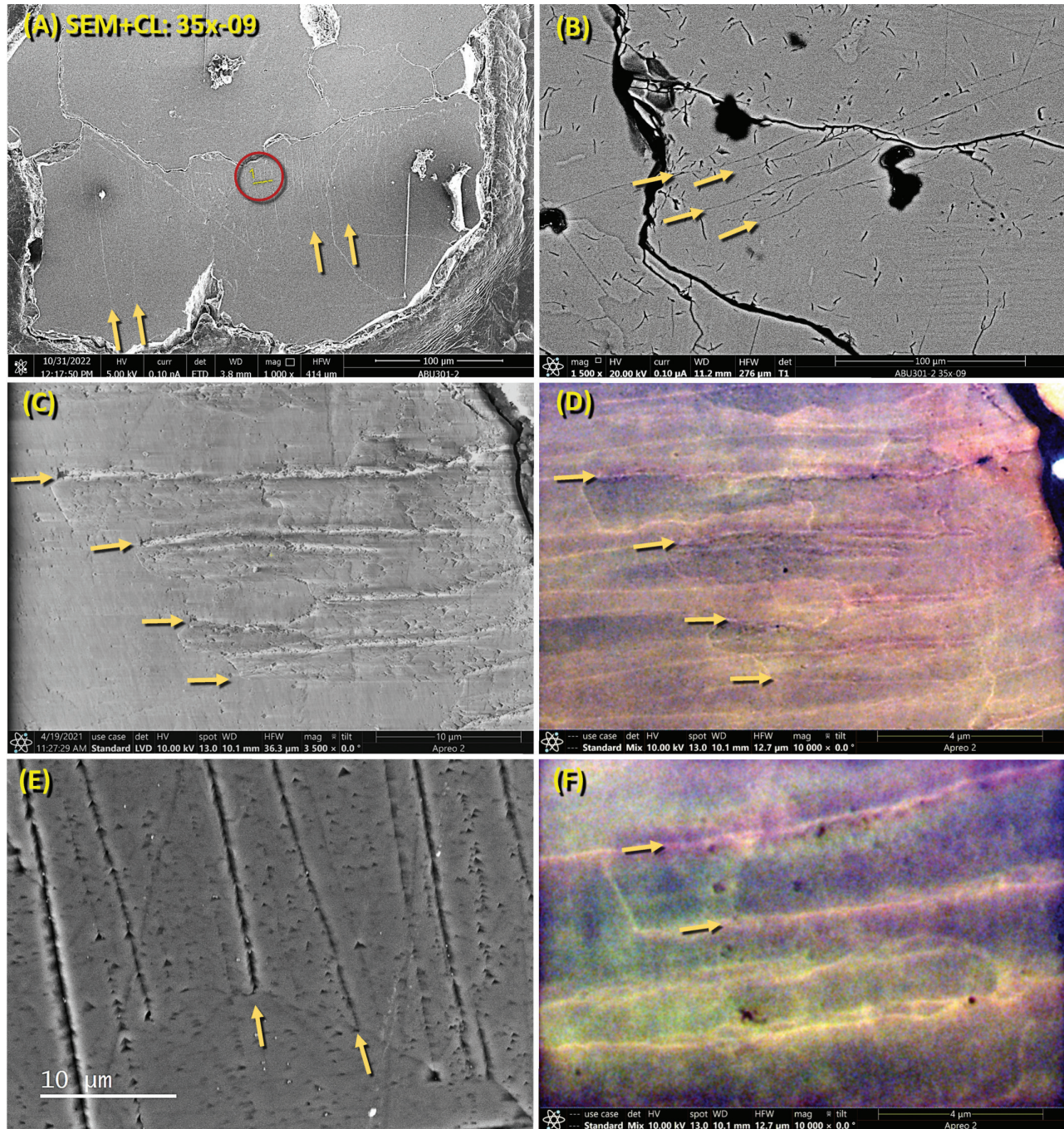


Figure 3: SEM and cathodoluminescence [CL] images of shock fractures in Abu Hureyra quartz grain 35x-09. (A) SEM-BSE image of shock-fractured grain. Gold arrows point in the direction of selected fractures. The red circle marks the lift-out location for focused ion beam milling. (B) Close-up SEM-BSE image of the same grain. Gold arrows point in the direction of selected fractures. (C) Close-up SEM-BSE image with gold arrows marking selected open fractures. (D) CL image of approximately the same area as in panel C. The dark-red-and-black colors signify the presence of open fractures containing amorphous silica, as reported in studies by Hamers et al. [16, 73–75]. The generally reddish color of the quartz matrix cysts signifies that it was likely partially to fully melted and then recrystallized. (E) SEM-BSE image showing open fractures exposed by HF etching. (F) Close-up CL image. This grain is from YDB sample E301, 405 cm depth.

lamellae may luminesce red but not black [16, 73–75]. In contrast, non-shocked quartz lattice under CL often luminesces blue but not black [16, 73–75].

Transmission electron microscopy (TEM) [10]

Images acquired using high-resolution TEM show sub-planar shock fractures containing thin bands of amorphous

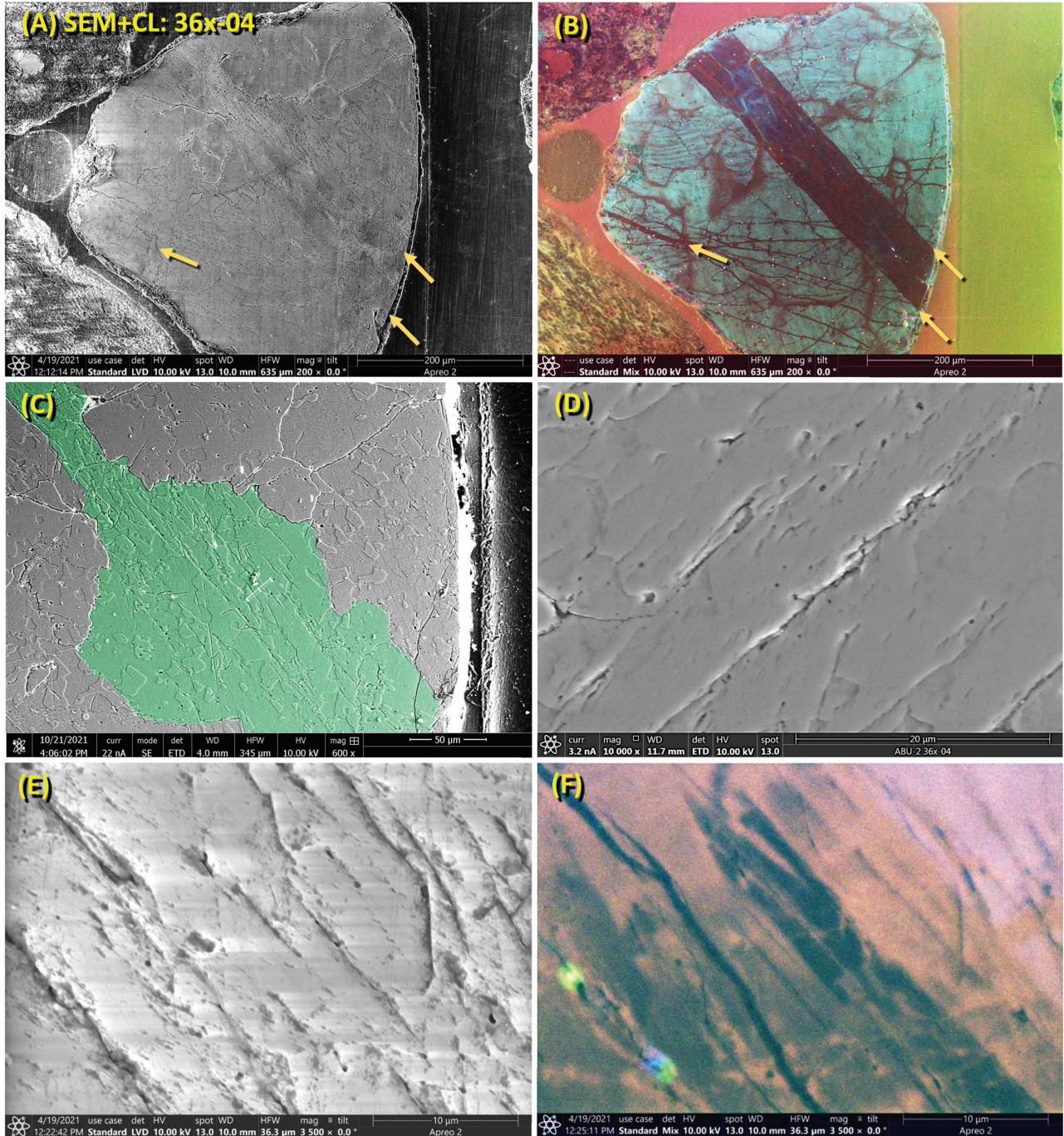


Figure 4: SEM and cathodoluminescence (CL) images of shock fractures in Abu Hureyra quartz grain 36x-04. (A) SEM-BSE image of polycrystalline quartz grain. Shock fractures at arrows. (B) CL image of the same area of the grain in panel A. The righthand two arrows mark a wide, dark-red-and-black area indicative of amorphous silica, confirmed by TEM. (C) SEM-BSE image of quartz with fractured subgrain high-lighted in green. (D) Close-up SEM-BSE image showing open shock fractures, as exposed by HF etching. (E) Another SEM-BSE image shows open shock fractures. (F) CL image of the same area shown in panel E. Note that shock fractures are filled with non-luminescent black material, indicative of amorphous silica. This grain is from YDB sample E301, 405 cm depth.

silica (Figures 5–9). Numerous filled inclusions or vesicles often contain glass or gases and are closely associated with shock fractures (Figures 5–7). Madden et al. [77] reported that multi-phase inclusions of glass, gases, and fluids are

typical at Meteor Crater in sandstone lightly shocked at ≥ 5.5 to 13 GPa. In contrast, that study observed no multi-phase inclusions in samples formed at >13 GPa, suggesting that at Abu Hureyra, the fractures and inclusions formed at <13

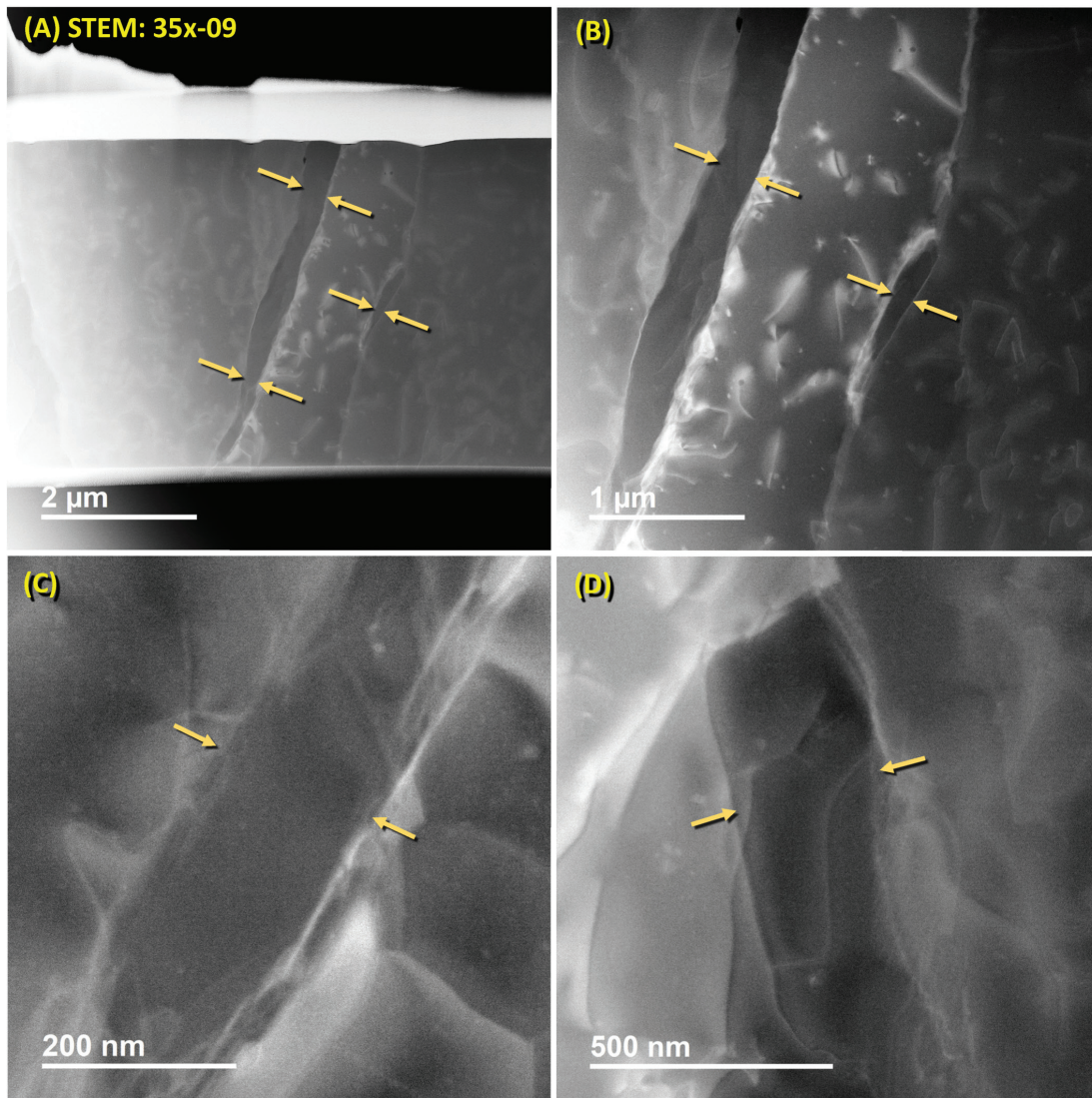


Figure 5: Scanning-transmission electron microscopy (STEM) images of Abu Hureyra shock-fractured quartz grain 35x-09. (A) Bright-field STEM image shows a glass-filled fracture between the gold arrows at the left. Right arrows mark a smaller glass-filled area. Glass filling was confirmed using other procedures documented below. (B) Close-up of the middle part of the grains shown in panel A. (C, D) Close-up images showing glass filling the areas between the gold arrows. This grain is from YDB sample E301, 405 cm depth.

GPa [77]. In contrast, unshocked tectonically-deformed quartz grains may display lines of bubbles, known as decorations, that form by the dissolution of quartz by water rather than by shock-related processes.

Selected area diffraction (SAD) [10]

This crystallographic technique is performed using TEM. When the TEM's electron beam passes through a quartz grain, it sometimes produces a diffuse halo with a d-spacing of ~ 1.23 Å (Figure 7), characteristic of amorphous quartz.

High-resolution TEM [10]

This TEM process allows the high-magnification observation of the structure in a crystal's lattice. Thus, the technique

can detect the presence or absence of amorphous silica, as seen in Figures 8 and 9.

Fast-Fourier transform (FFT) [10]

This study's FFT analyses commonly displayed crystalline structures up to hundreds of nanometers away from the shock fractures. However, FFT images revealed that most shock fractures contain a diffuse halo or ring indicative of amorphous material [29, 75, 78], especially in the thin bands of glass along the shock fractures. FFTs of the material filling these thin fractures display the diffuse halo-like patterns characteristic of amorphous material [29, 75, 78] with d-spacings of ~ 3.50 and ~ 3.70 Å (Figures 8 and 9). This amorphous silica is commonly heterogeneously mixed with

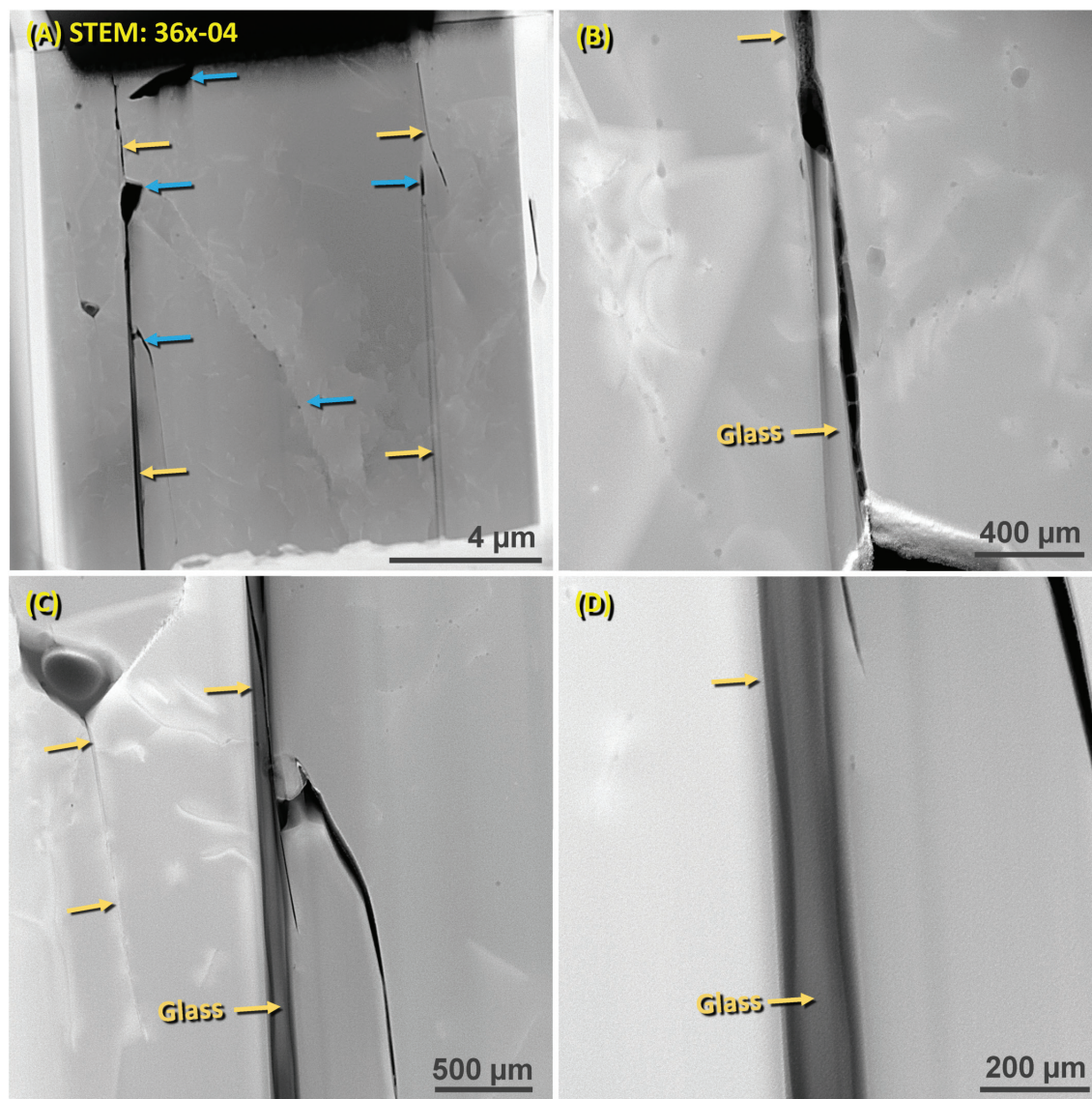


Figure 6: Scanning-transmission electron microscopy (STEM) images of Abu Hureyra quartz grain 35x-09. (A) Bright-field STEM image shows gold arrows indicating two sub-planar, sub-parallel glass-filled fractures. Blue arrows mark voids and vesicles in the quartz. Glass filling was confirmed by using other procedures, as documented below. (B) Close-up of right-hand shock fracture shown in panel A. (C, D) Close-up images with arrows indicating amorphous glass. This grain is from YDB sample E301, 405 cm depth.

crystalline quartz for several hundred nanometers on each side of the fractures.

Gleason et al. [79] conducted experiments on amorphous silica and noted that unshocked amorphous silica had a d-spacing of about 4.20 Å. In contrast, quartz exposed to shock pressures ranging from 4.7 to 33.6 GPa transformed into amorphous silica that permanently densified, causing the standard glass d-spacing to decrease within a range of 3.36 to 4.00 Å. Thus, our study's mean d-spacing values of 3.60 Å are consistent with Gleason's range, supporting the interpretation that amorphous silica from Abu Hureyra was shocked and possibly densified at high pressures ≥ 4.7 GPa.

Energy dispersive spectroscopy using SEM (SEM-EDS) and TEM (TEM-EDS) [10]

For these analyses, we selected multiple areas that displayed fractures filled with material (Figures 10–14). TEM-EDS and SEM-EDS analyses revealed that the material filling the fractures is predominantly composed of silicon and oxygen (range: 98–99 total wt%). The wt% values of oxygen (14 to 48 wt%) were typically below the stoichiometric values of quartz (53 wt%). Together with the diffuse rings exhibited in the FFT results (Figures 7–9), this finding confirms that the material filling the fractures is amorphous silica.

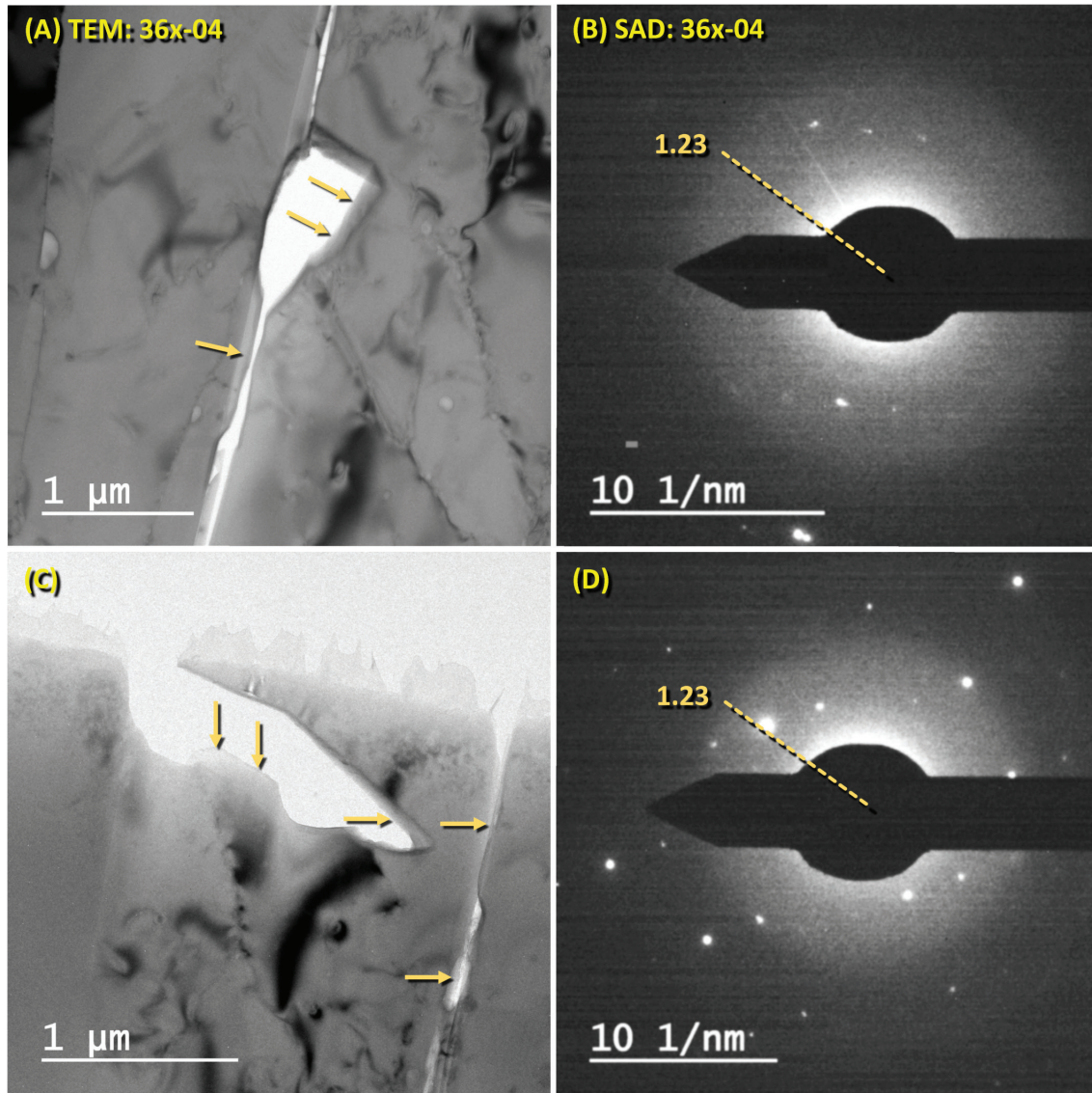


Figure 7: TEM and SAD images of quartz shock fractures filled with amorphous silica Abu Hureyra quartz from grain 36x-04. (A, C) TEM bright-field images of shock fractures. Arrows point to thin gray bands of amorphous silica. White areas represent voids and vesicles along the fractures. (B, D) SAD images showing diffuse rings indicative of amorphous silica. D-spacings of 1.23 Å are typical for the outer edge of the diffuse rings at the end of the dashed line. The grain is from sample E301.

Micro-Raman

Acquiring multiple points with a micro-Raman laser is an excellent method to identify potential crystallinity variations along selected quartz grain fractures. However, even after much polishing of the quartz grains, their extensive fracturing made it challenging to acquire Raman spectra. Nevertheless, the observation of low intensity (<3000 arbitrary units (a.u.)) of the Raman band at 466 cm^{-1} within the fractures, plus the appearance of an extra Raman band at 1330 cm^{-1} , suggests the presence of amorphous silica in the fractures with crystalline quartz on either side (Figure 15).

Electron backscatter diffraction (EBSD) [10]

Analyses performed using EBSD rely on varying comparisons of Kikuchi patterns. These are produced by the passage of the electron beam through the crystal, revealing the microstructural properties in a given grain. We used several EBSD routines, including a technique called “PRIAS,” an acronym for “Pattern Region of Interest Analysis System.” With this technique, each pixel in an EBSD pattern can collect light at small angles relative to the incident beam, thus allowing one to infer differing angles of the crystalline structure. The images produced by EBSD reveal an extensive network of oriented shock

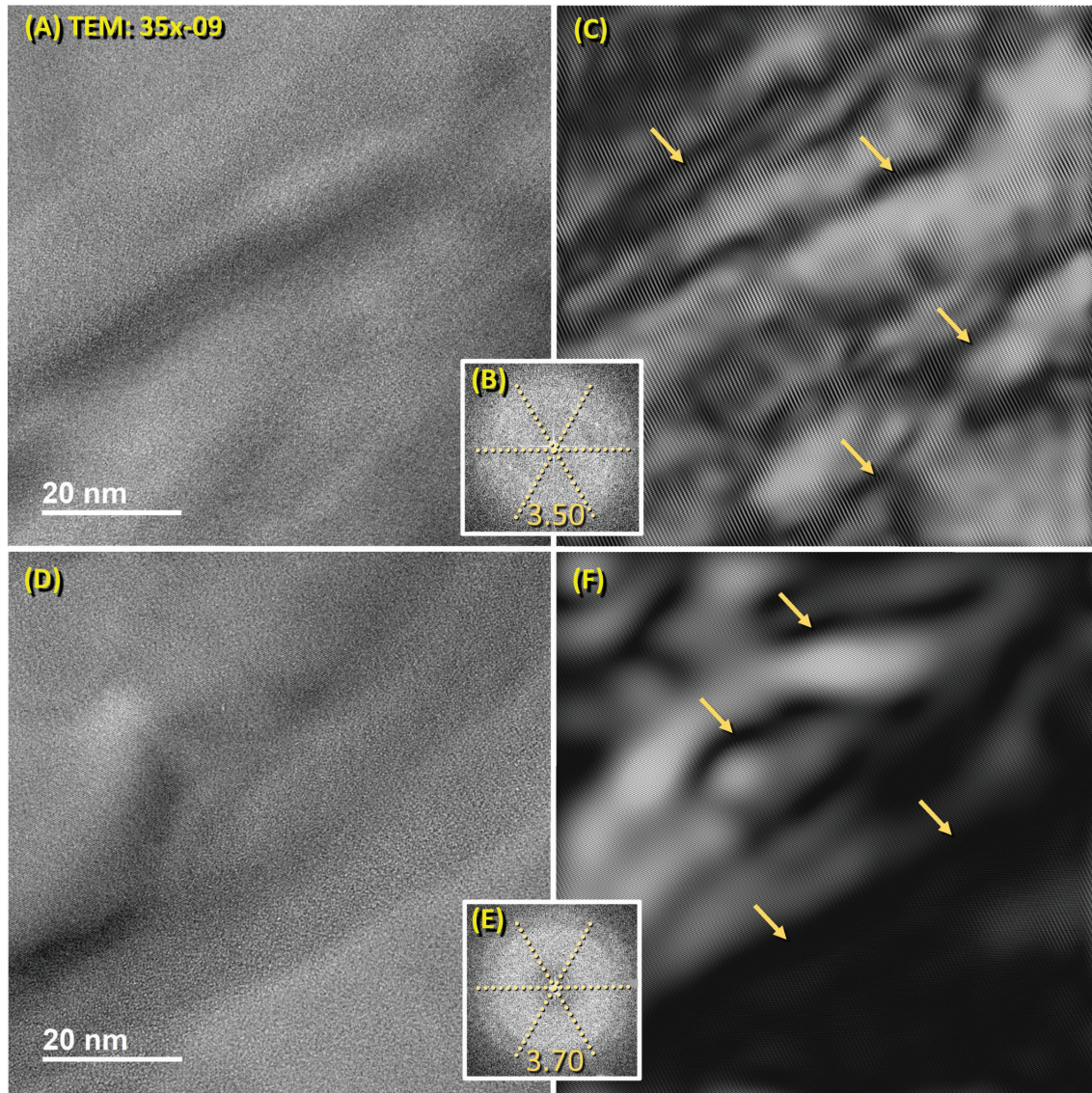


Figure 8: High-resolution Transmission electron microscopy (TEM) images of shock-fractured quartz grain 35x-09 filled with amorphous silica. (A, D) The high-magnification image shows the oriented texture of quartz grain. Crystalline lattice is visible in some areas but not in others. (B, E) Fast-Fourier Transform (FFT) image of the region represented by panel A. These FFT images exhibit a diffuse halo with respective d-spacings of 3.50 and 3.70 Å, indicative of the presence of amorphous silica. (C, F) Inverse Fast-Fourier Transform (IFFT) derived from spot diffraction patterns in full FFT image (not shown). The fields of view shown in the lefthand panels are the same as in the righthand panels. Lighter areas represent fully crystalline quartz, and dark areas represent damaged crystalline lattices containing some amorphous silica, as confirmed by FFT and selected area diffraction (SAD). This grain is from YDB sample E301, 405 cm depth.

fractures for some quartz grains in sample E301 from Abu Hureyra (Figures 16 and 17).

EBSD “image quality” superimposed by “local orientation spread”

The high pressures during shock metamorphism damage and distort the crystalline lattice of quartz grains. To identify and quantify any potential grain damage, we used an EBSD routine called “local orientation spread” that generates Kikuchi patterns of the quartz lattice. The EDAX EBSD software

compares these short-range patterns to reveal possible rotations or misorientations of the crystalline lattice, after which the average misorientation of any given point is calculated relative to neighboring points. In sample E301 from Abu Hureyra, we observed values ranging from 0° to $\sim 5^\circ$ of misorientation and observed that this misoriented lattice tends to be concentrated along the shock fractures (all panels in Figures 16 and 17). We found that such misorientations are common in quartz with shock fractures but are typically not in unshocked natural quartz grains.

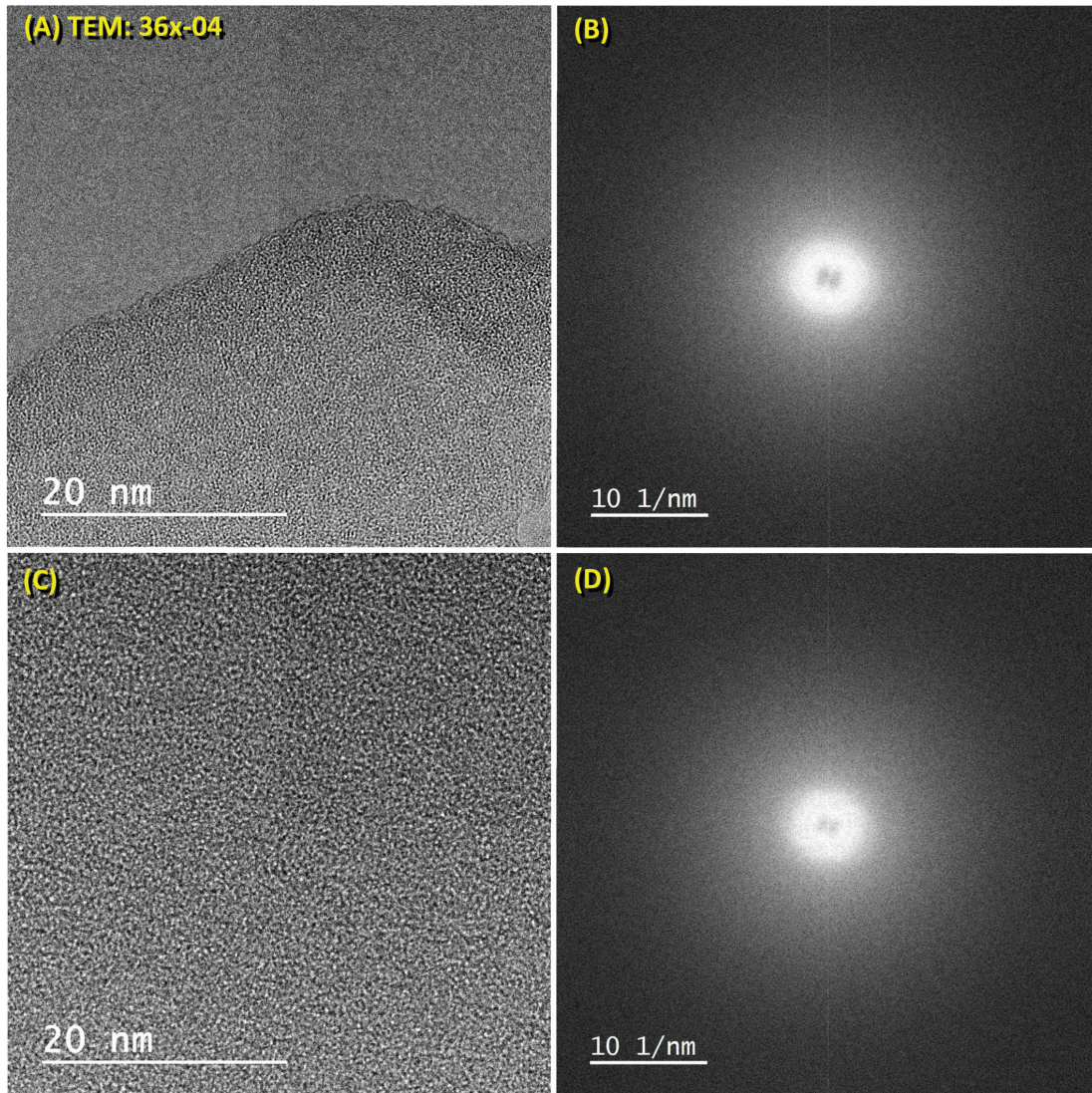


Figure 9: High-resolution TEM images of shock-fractured quartz grain 36x-04. **(A)** High-magnification image of the region of interest in quartz grain. The upper portion of the image is an open void. The lower part shows a short-range ordering of atoms without evidence of crystalline structure. **(B)** The FFT image of the left panel displays no diffraction spots indicative of crystalline structure. Instead, the bright center indicates the diffuse glow produced by amorphous silica. **(C)** High-magnification image of a region of interest in quartz grain. The image shows a short-range ordering of atoms without evidence of crystalline structure. **(D)** The FFT image of the left panel displays no diffraction spots indicative of crystalline structure. This grain is from YDB sample E301, 405 cm depth.

EBSD “grain reference orientation deviation” values superimposed on EBSD “image quality” values

Orientation deviation maps (Figures 16 and 17) assist with visualizing the distribution of local lattice angular misorientations by color-coding the variations. EDAX’s EBSD software analyzes and colorizes individual points to illustrate any rotation of the crystalline lattice around an arbitrary common point on the grain. The software uses multiple colors to represent areas with different short-range misorientations relative to a common point. In contrast, unshocked grains and tectonically-deformed grains display few misorientations.

EBSD “inverse pole Figure” values superimposed on EBSD “image quality” values

These Figures (Figures 16 and 17) reveal variations in the lattice axes of quartz relative to a frame of reference, which, in these examples, is the (0001) basal plane. In each case, measurements show that some quartz grains are composed of merged crystals known as Dauphiné twins that are rotated 60° relative to each other around a common *c*-axis. Dauphiné twinning is undetectable by standard optical microscopy and SEM backscatter electron imagery (SEM-BSE) but can easily be seen using EBSD. These twins are commonly found randomly distributed in many quartz grains, but in

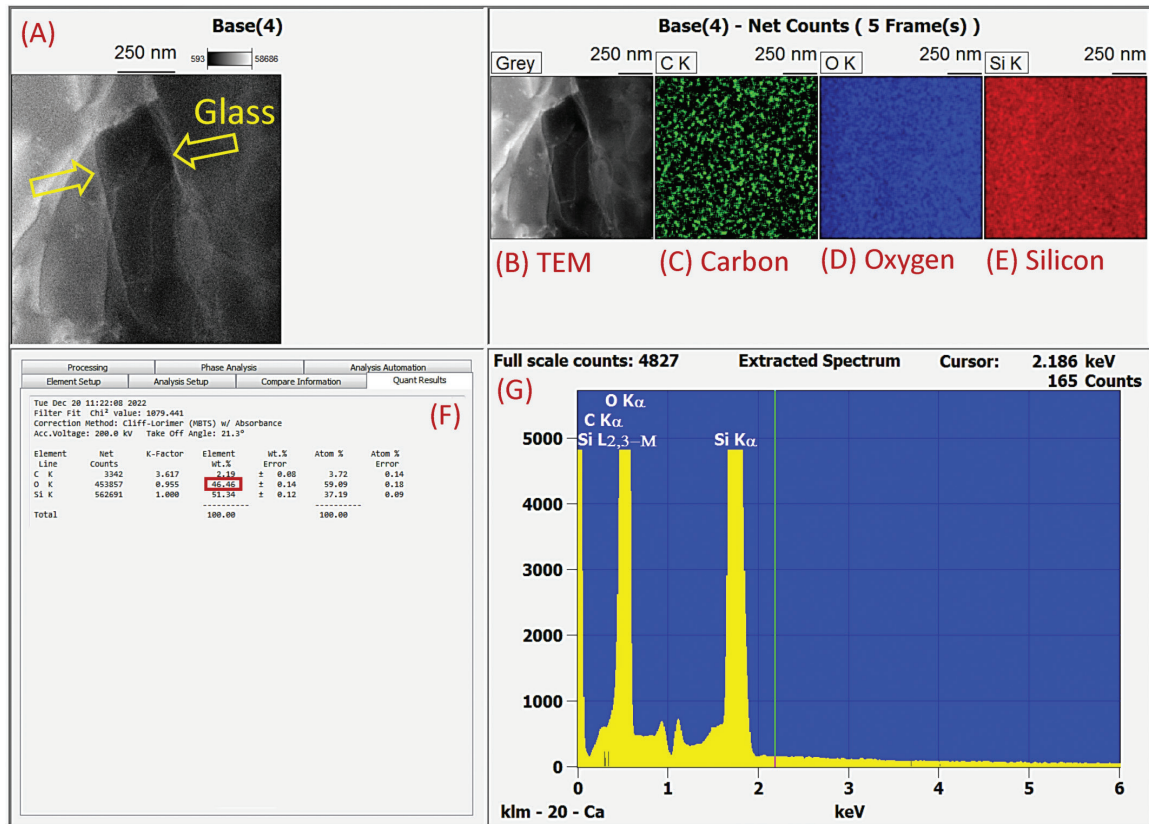


Figure 10: TEM-EDS of shock-fractured quartz grain 35x-09. 98 wt% SiO₂ with a trace of carbon contamination on the surface. Oxygen is at 46 wt%, slightly below EDS uncertainty of ±10 wt%.

shock-fractured quartz, they are frequently closely aligned with the fractures, suggesting that the grain first fractured and melted, after which it recrystallized as a Dauphiné twin oriented approximately parallel to the fracture pattern.

Our analyses indicate that although Dauphiné twins are nearly ubiquitous in all quartz grains, they are typically distributed randomly in unshocked or tectonically deformed grains. In contrast, for the shock-fractured quartz identified in our study, Dauphiné twins typically align with the trend of the shock fractures, suggesting that they crystallized when the fractures formed under high stress or cooled from high temperatures. It has long been recognized that Dauphiné twins form when quartz is subjected to mechanical stress [80]. Subsequently, Wenk et al. [81] further concluded that Dauphiné twinning forms under high thermal and mechanical stress and later [82] reported that Dauphiné twinning provides evidence for an impact-related origin of shocked quartzite collected from the Vredefort crater in South Africa.

Discussion

Our multiple analyses have revealed the potential presence of fractured quartz grains limited to the YDB cosmic

impact layer in the Abu Hureyra section. It is important to note that this dark layer had previously been identified by Moore et al. [1, 35–38] based on abundance peaks in nanodiamonds, magnetic micro-spherules, high-temperature meltglass, carbon micro-spherules, platinum, nickel, cobalt, chromium, and other potential impact-related proxies [35, 37, 58] as summarized in Figure 18. This assemblage of inferred impact-related proxies and the size characteristics of specific proxies, such as meltglass, implies the presence of a nearby cosmic impact [1, 2, 37]. Although no known crater is near Abu Hureyra, the impact hypothesis does not require one. Most of the same inferred proxy evidence observed at Abu Hureyra has been found at accepted impact events with no known confirmed craters, including the Dakhleh Oasis in Egypt [83], the Australasian tektite field in SE Asia [35], and the Atacama Desert [84].

We now discuss the potential processes of formation and origin of the fractured quartz grains identified in the YDB cosmic impact layer at Abu Hureyra. This discussion is critical because the features exhibited in the YDB shock-fractured quartz grains most likely formed at relatively low pressures. Because tectonic lamellae also form at relatively low pressures, it is crucial to differentiate those from cosmic airbursts and crater-forming impacts.

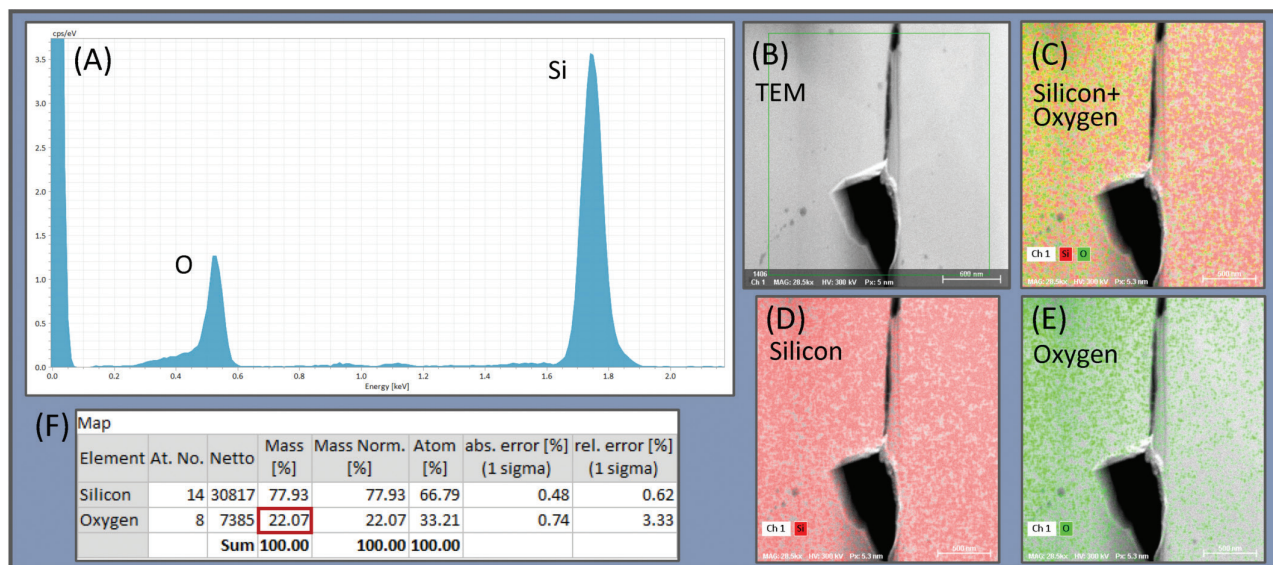


Figure 11: TEM-EDS of shock-fractured quartz grain 36x-04. 100 wt% SiO₂. The area of the grain is highly depleted in oxygen at 22 wt%. Based on the stoichiometric ratio of quartz, this suggests a mixture of ~41 wt% SiO₂ with ~59% native Si in the area analyzed.

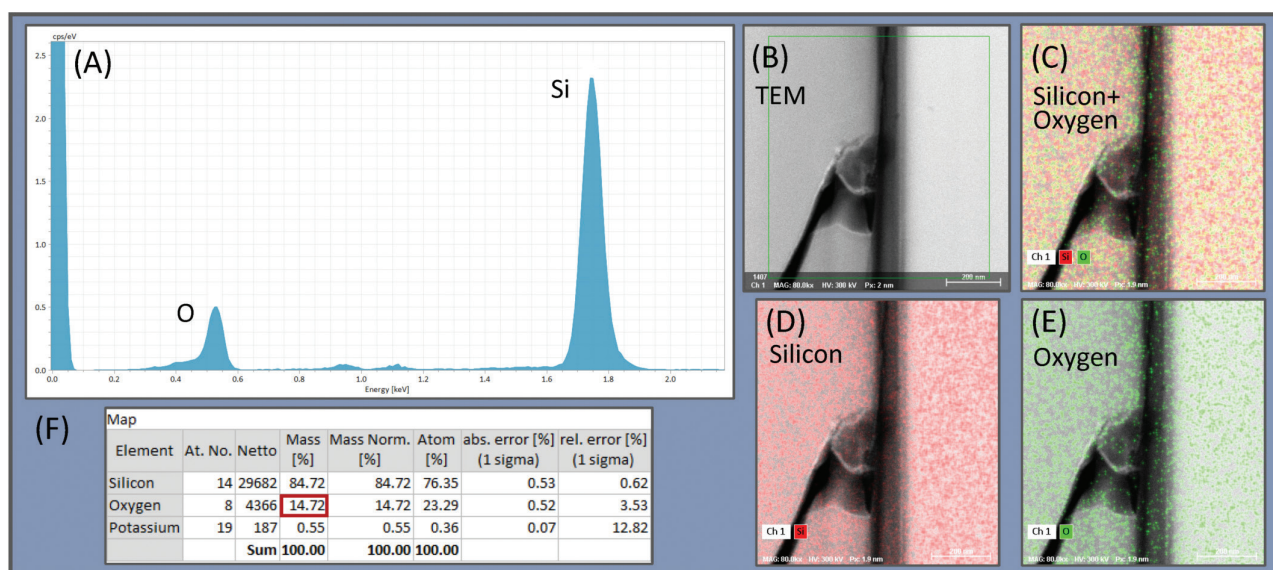


Figure 12: TEM-EDS of shock-fractured quartz grain 36x-04. 99.4 wt% SiO₂. The area of the grain is highly depleted in oxygen at 14.7 wt%. Based on the stoichiometric ratio of quartz, this suggests a mixture of ~27.6 wt% SiO₂ with ~71.8 wt% native Si in the area analyzed.

Production of fractures containing amorphous silica. Several laboratory experiments have investigated the impact-related shock transformation of quartz to amorphous silica at minimum pressures of <6 GPa (as discussed in Hermes et al. [10]). However, it appears that no previous experiments have been conducted on unconsolidated quartz grains as in our investigation but rather, were only done on tightly constrained large crystals or milled cylinders of quartz. None of the following studies are analogous with the relatively unconsolidated quartz grains characteristic of the YDB sediments at Abu Hureyra.

- Kieffer [28] analyzed shocked sandstone from Meteor Crater and concluded that impact-related, glass-filled fractures began to form at 5.5 GPa but not at lower pressures (Table 2).
- Christie and Ardell [12] performed shock compression laboratory experiments on large quartz crystals and noted amorphous silica glass filling the fractures at a confining pressure of 1.5 GPa.
- Kenkmann et al. [85] performed shock experiments on 1.5-mm-wide cylindrical samples of quartz. Using moderate shock pressures of 6–34 GPa, they could

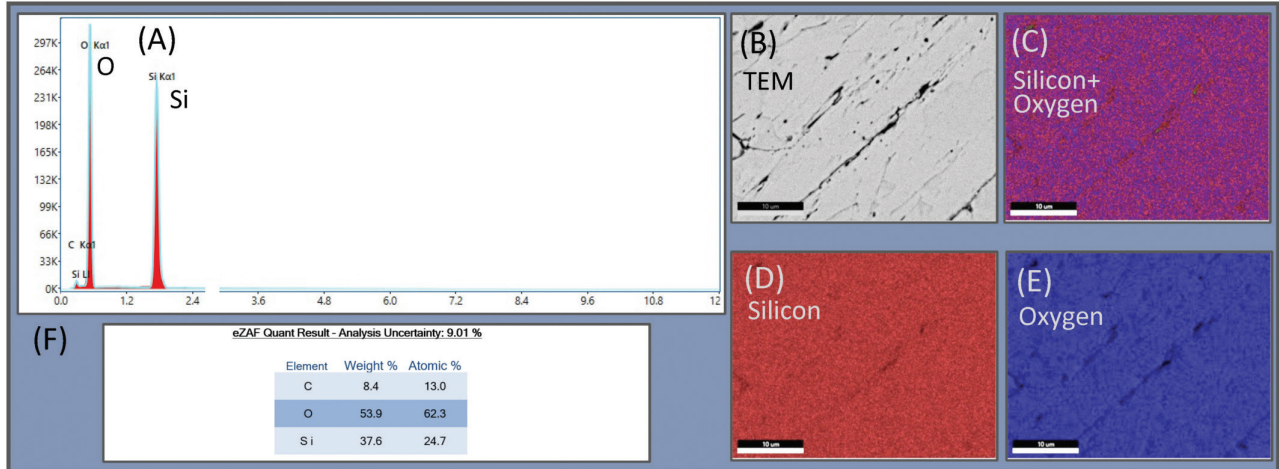


Figure 13: TEM-EDS of shock-fractured quartz grain 36x-04. 91.6 wt% SiO₂ with 8.4 wt% C across the field of view.

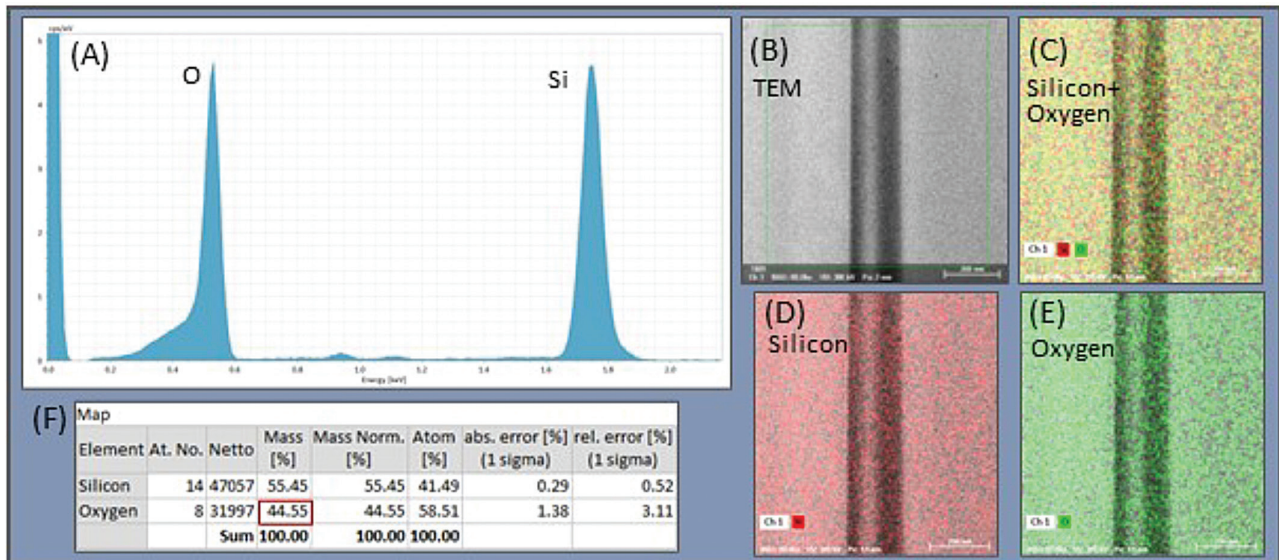


Figure 14: TEM-EDS of shock-fractured quartz grain 36x-04. 100 wt% SiO₂. Oxygen is at 44.55 wt%, slightly below the EDS uncertainty of ±10 wt%.

generate veins of amorphous silica that were 1–6 μm wide.

- Kowitz et al. [4, 8, 34] conducted detailed laboratory experiments to determine the lower pressure limit for forming shock features called “sub-planar, intra-granular fractures.” [4] In their experiments, a steel plate was explosively driven into cylinders of quartz-rich sandstone at pressures of 5, 7.5, 10, and 12.5 GPa. Visible shock fractures and amorphous silica (~1.6 wt%) first appeared at 5 GPa [4], similar to the results of Kieffer [28]. See Table 3.
- In quartz grains experimentally shocked at 5 to 17.5 GPa, Fazio et al. [88] observed glass veins composed of

amorphous silica extending several microns in length and generally thicker than 50 nm.

- Wilk et al. [89] found amorphous silica in experimentally shocked rocks called shatter cones that formed at low shock pressures of 0.5–5 GPa.
- Laboratory shock experiments by Martinelli et al. [90] produced intra-granular fractures in quartz crystals with a minimum diameter of 3400 μm, larger than any we examined. The fracturing process reportedly produced amorphous silica composed of low-temperature nanocrystalline cristobalite, which was not observed in the fractures of our study. The reported compression applied was as low as 0.2 GPa; the maximum compression is unclear.

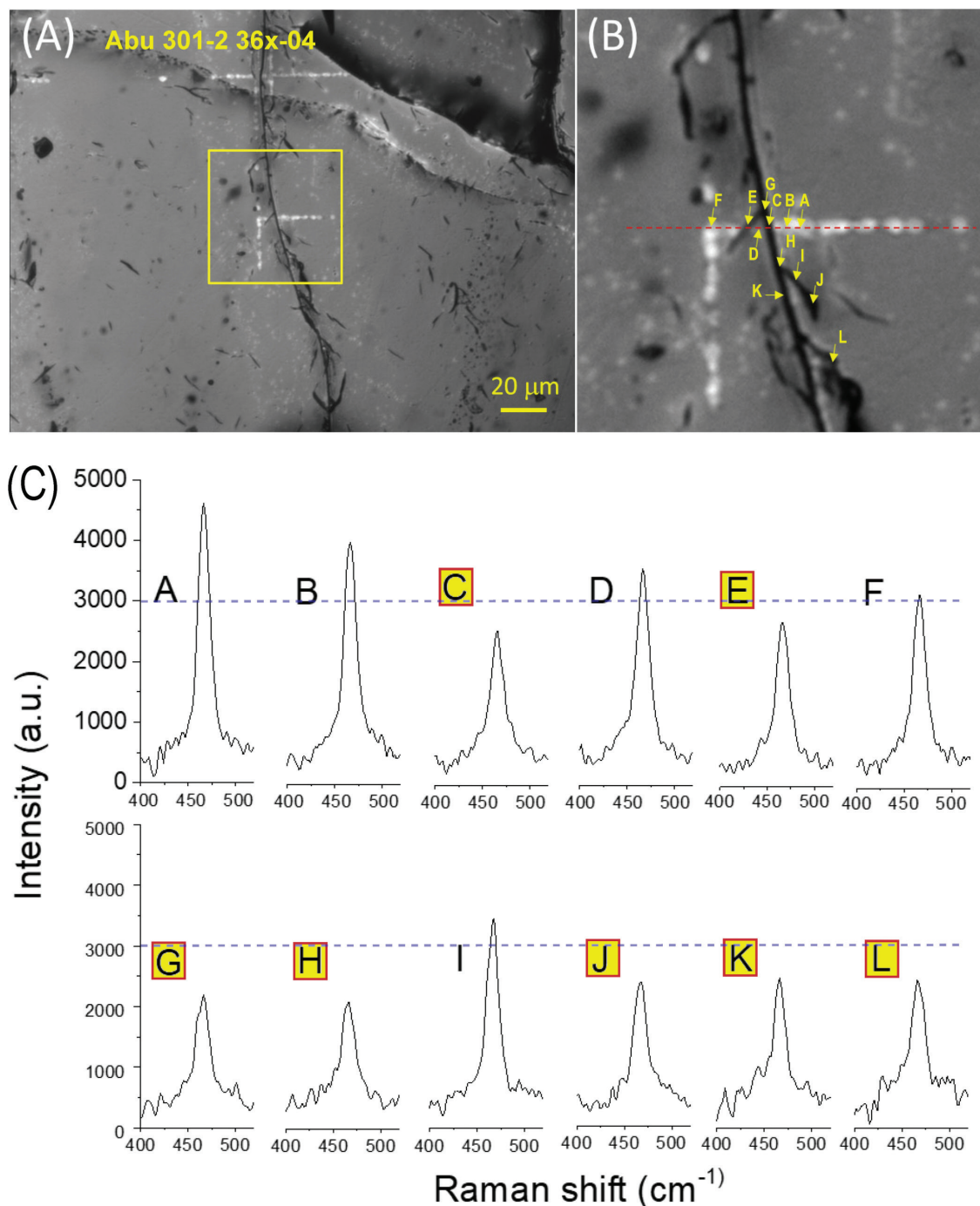


Figure 15: Micro-Raman for shock-fractured quartz Abu Hureyra grain 36x-04. (A) Bright-field SEM image. The yellow square marks the area investigated. (B) Close-up of the yellow square in panel A. (C) Micro-Raman spectra of grain at positions A through L. Crystal quartz Raman band at 466 cm^{-1} was observed at all positions. The intensities marked with yellow letters are all less than 3000 a.u., interpreted as indicating the presence of amorphous silica.

In summary, these laboratory studies report the formation of amorphous silica in fractures produced by shock pressures averaging 4.2 GPa (range 0.2 to 10 GPa), with five of the eight studies reporting >5 GPa as a minimum observed pressure. No experimental study has ever reported glass-filled fractures in natural unshocked quartz grains, nor have they

been observed in nature from any non-impact process [10, 14]. In contrast, Ernstson et al. [91] have reported extensive glass-filled fracturing in cosmic impact events during the Cenozoic.

Regarding the importance of amorphous silica in studies of impact-shock metamorphism, French and Koeberl [20]

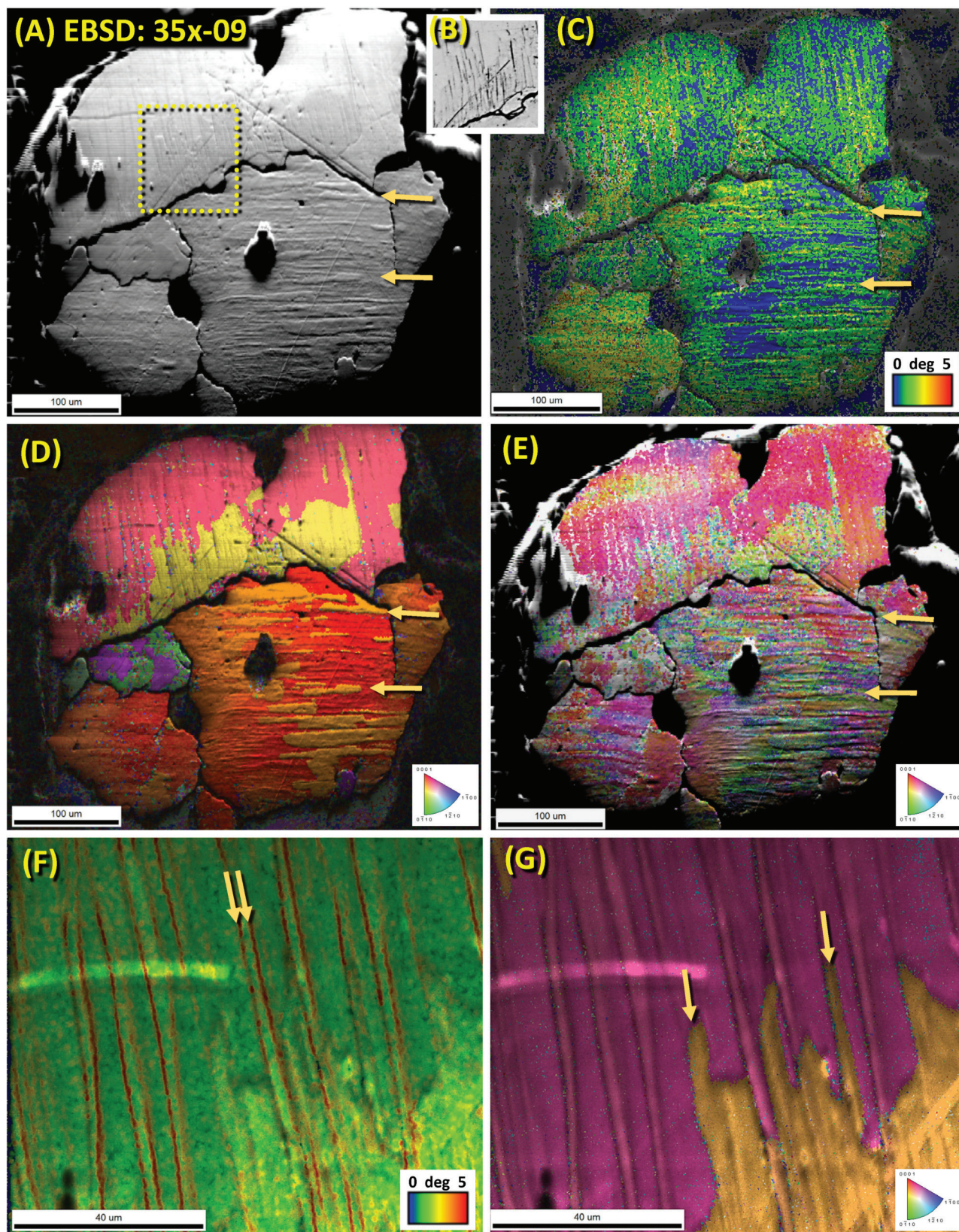


Figure 16: Images of Abu Hureyra shock-fractured quartz grain 35x-09 using Electron Backscatter Diffraction (EBSD). (A) EBSD image reveals fractures at arrows. The largest fractures represent sub-grain boundaries. (B) Epi-illumination microscopy (EPI) image of the yellow box in panel A exhibits fractures. (C) EBSD Figure of "image quality" (IQ) is overlain by "local orientation spread" (LOS), illustrating the

← degree of damage to grain. The scale at the lower right of panel C represents degrees of misorientation from 0° (blue) to 5° (red). The greatest misorientation (i.e., damage) is concentrated along shock fractures. **(D)** “Inverse pole Figure” (IPF) values superimposed on IQ values, showing misorientation. The inset displays color-coded Miller-Bravais crystallographic indices. Within each sub-grain, the two primary colors represent Dauphiné twinning. **(E)** Image acquired using the PRIAS technique overlain by “grain reference orientation deviation” (GROD), showing many misorientations. Index key at lower right. **(F)** Close-up image of LOS superimposed on IQ. Fractures typically display twin sub-parallel tracks. **(G)** Close-up image of IPF over IQ.

stated that “*amorphous or ‘glassy’ phases ... constitute another set of unique and distinctive criteria for the recognition of shock-metamorphosed rocks...*” Similarly, Bohor et al. [13] stated that “*the formation of quartz glass within fractures ... allows a definitive distinction ... between these shock PDFs and the glass-free dislocation trails marking slow tectonic deformation.*”

Sources for amorphous silica (glass). We now consider alternate possibilities for forming amorphous silica, including whether the glass might be hydrated silica (opal, hyalite), which commonly precipitates onto quartz grains. However, this study’s glass is inconsistent with hydrothermal quartz, hyalite, opal, or melted silicious plant material. This inconsistency is because the filling lacks spherical micro-structures often present in opal [92] and because TEM-EDS analyses reveal insufficient oxygen levels to account for silica’s hydration [92], typically ~66 wt% oxygen. Instead, we observed oxygen concentrations of ~14 to 48 wt% for the glass in the YDB samples, too low to represent hydrated silica. For all shock-fractured grains analyzed, the wt% of oxygen was less than 53 wt%, the stoichiometric value for quartz, indicating that the grains would have experienced a sequence of events following exposure to high temperatures: i.e., they melted, the quartz dissociated, oxygen was driven off, native silica was left behind and mixed with SiO₂, and then cooled under oxygen-deficient conditions. This result is consistent with the known sequence of cosmic impact events.

The material filling the fractures is not chalcedony, agate, or onyx because these are microcrystalline forms of quartz with textures easily detected using high-resolution SEM and TEM. Similarly, the filling is not chert or flint, which are forms of cryptocrystalline quartz, because TEM and SEM analyses would reveal visible texturing, and we found none.

Lamellae in tectonically deformed quartz may resemble shock fractures. However, Gratz et al. [14] reported that glass has never been observed in tectonically deformed quartz grains (J. Christie, personal communication in Gratz et al. [14]). Bohor et al. [13] also concluded that the formation of quartz glass within fractures caused by high-strain-rate shock waves associated with impacts is distinctively different from the glass-free dislocations marking slow tectonic deformation. Likewise, Hermes et al. [10] reported that one of the co-authors of that study (H.-R. Wenk) had performed multiple analyses of tectonic lamellae and never observed

amorphous silica associated with tectonic lamellae in quartz grains [81, 82, 92–95].

We also considered whether it might be possible that these fractured quartz grains are intrusive from an older or younger cosmic impact event. However, they were not found above or below the 12,800-year-old YDB layer at Abu Hureyra, making it unlikely that they are from a different event. In addition, the excavation trench was atop a large mound, making it unlikely that the grains were redeposited upslope by erosion of older sediments during the early Younger Dryas.

Potential formation mechanisms. There are several possible mechanisms for glass-filled fractures that are not mutually exclusive, including grain-to-grain collisions, shockwave pressures that exceed the compressive strength of the grains, intra-grain reflected pressures that exceed the tensile strength of the grains, and rapid thermal expansion followed by rapid quenching.

In a previous study, Kieffer et al. [29] proposed the formation of glass-filled fractures through a process called “jetting,” in which molten quartz is injected under high temperature, pressure, and velocity into the fractures in quartz grains. For silica to be forced into the fractures, both pressures and temperatures must be very high. Such conditions are common in cosmic airbursts and impact structures but not during other natural processes.

Ernstson [33] conducted low-shock experiments with 6-mm plastic projectiles at 1250 m/s impact velocity fired into glass rods. He observed extreme tensile fragmentation by spallation, defined as the sum of effects related to rarefaction waves in quartz grains during a cosmic impact event. During spallation, compressive shock waves enter a quartz grain, intersect an internal grain boundary, and are then reflected as a rarefaction pulse. If the reflected tensile stress exceeds the tensile strength of the quartz grain, the shock wave produces tensile fractures roughly perpendicular to the shock direction. Because the tensile strength of quartz is much lower than its compressive strength, tensile fracturing and spallation frequently cause the most mechanical damage to a quartz grain. Distinct glass-filled shock fractures in quartz grains as the result of shock spallation were first reported for impactites from the Bronze Age/Iron Age Chiemgau impact [33, 96, 97] and later from shocked impact melt rocks in the Pleistocene/Holocene Saarlouis/Nalbach impact event [91]. In both cases, the glass penetrated from outside the shocked cobbles into the open spallation fractures.

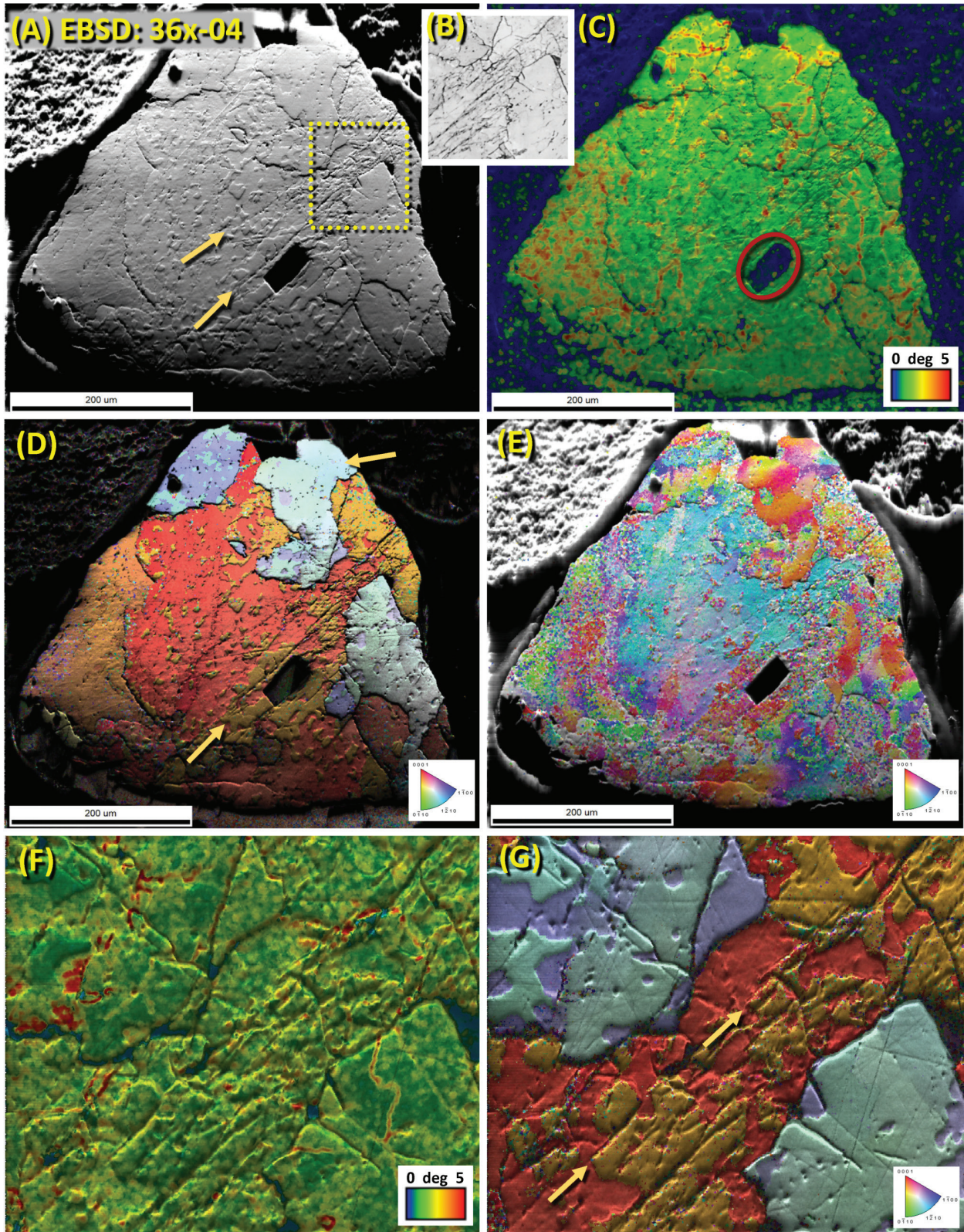


Figure 17: Abu Hureyra shock-fractured quartz grain 36x-04. (A) The PRIAS technique image reveals fractures. (B) EPI image of the yellow box in panel A exhibits fractures. (C) LOS over IQ (image quality) shows the degree of misorientation. Color key at the bottom right. The red circle marks the FIB foil extraction site. (D) IQ over IPF shows misorientation. Inset indicates color-coded Miller-Bravais indices. The two primary colors represent Dauphiné twinning. (E) GROD under PRIAS shows a wide range of misorientations, consistent with melting followed by partial recrystallization. (F) Close-up of LOS over IQ. (G) Close-up of IPF over IQ. See the caption for Figure 16 for abbreviations.

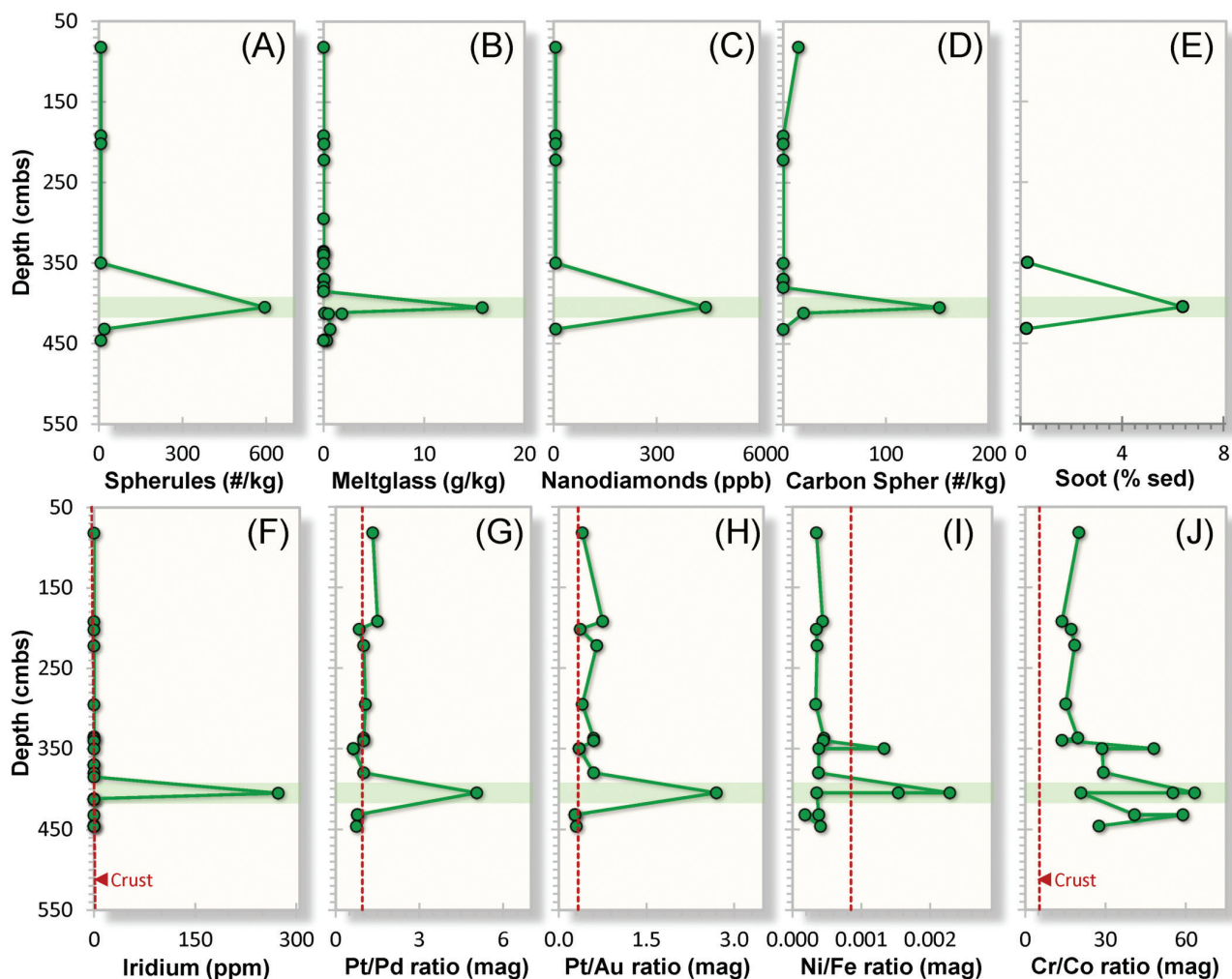


Figure 18: Compilation of peak concentrations of various impact-related proxies in the YDB layer at Abu Hureyra. (A) Ca-Si-rich and Fe-rich micro-spherules; (B) high-temperature meltglass; (C) nanodiamonds; (D) carbon micro-spherules produced by biomass burning; (E) black carbon or soot in sediment produced by biomass burning; (F) iridium; (G) platinum/palladium (Pt/Pd) ratio; (H) platinum/gold (Pt/Au) ratio; (I) nickel/iron (Ni/Fe) ratio; and (J) chromium/cobalt (Cr/Co) ratio. The elemental peaks suggest the influx of additional amounts of non-local Ir, Pt, Ni, and Cr. The main peaks in the green horizontal bar represent the YDB layer (sample E301) with a Bayesian-model radiocarbon age of $12,800 \pm 40$ cal BP. All YDB elemental abundance peaks are substantially larger than background concentrations and average abundances for Earth's upper continental crust, marked "Crust" at the red dashed line. The plots are adapted from Moore et al. [1, 37] and are usable under Creative Commons, CC by 4.0 (<http://creativecommons.org/licenses/by/4.0/>).

Table 3: Shock stages in sandstones.

Shock stage	Range, low (GPa)	Range, high (GPa)	Lithology
0	≤ 0.2	0.9	Undeformed, porous sandstone
1a	0.9	3	Compacted, porous, deformed sandstone
1b	3	5.5	Compacted, non-porous, deformed sandstone
2	5.5	13	Dense sandstone with 3 to 10 wt% glass and <95% quartz
3	13	39	Dense sandstone with up to 20 wt% glass and 45 to 80 wt% quartz
4	>30	–	Dense sandstone with 20 to 75 wt% glass and 15 to 45 wt% quartz
5	–	–	Vesicular rock with 80 to 100 wt% glass and up to 15% quartz

According to shock experiments by Kieffer et al. [28, 29] (Table 3), glass begins to appear in shock-fractured quartz in sandstones only at pressures ≥ 5.5 GPa, although fractures form without glass filling at lower pressures. These data are from Kowitz et al. [4], based on Kieffer [28, 29] and modified by others [86, 87].

In laboratory experiments, Martinelli et al. [90] concluded that fractures in quartz form rapidly in <50 ns not by compression but by tensional expansion produced by the reflected shockwave. They found that the fracturing process generates temperatures >1713°C, the melting point of quartz, thus producing amorphous silica along the fractures, as first proposed by Ernstson [33].

Few investigations have been conducted to characterize low- to moderate-pressure glass-filled shock fractures and lamellae. Currently, based on the available evidence and the above-cited studies (e.g., Kieffer et al. [29] and Ernstson [33]), molten silica or silica vapor may be injected into a quartz grain along several potential zones of weakness, including new fractures produced (i) by the impact shockwave; (ii) by the high temperatures of the airburst or impact; (iii) along pre-existing PDFs and PFs; (iv) along pre-existing tectonic lamellae; (v) along pre-existing subgrain boundaries; and (vi) along pre-existing quartz fractures. This shock fracturing process would overprint and modify any pre-existing features. Even though these different types of fractures may form under substantially different shock conditions, all have one common characteristic: amorphous silica is injected into them. Alternatively, high airburst/impact pressures may cause friction that produces amorphous silica, as is accepted for classical PDFs and PFs. In any event, further research is needed to understand the glass's formation process fully.

Conclusion

This investigation is the first to have identified and described shock-fractured quartz specific to the YDB cosmic impact layer at the onset of the Younger Dryas climate episode in the Abu Hureyra archeological site, thus verifying this as a cosmic impact layer. Using multiple high-resolution analyses, we observed that some quartz grains in the YDB layer are similar to those that Hermes et al. [10] reported for nuclear airbursts and Meteor Crater. These grains display fractures that:

- (i) Are either open or filled with amorphous silica glass;
- (ii) Are commonly oriented in the same approximate direction;
- (iii) Typically cross the entire quartz grain or sub-grain;
- (iv) Do not cross sub-grain boundaries;
- (v) Range from near-planar to curvilinear;
- (vi) Are commonly sub-parallel in orientation;
- (vii) Are often spaced less than a few microns apart;
- (viii) Usually range from less than one micron thick down to a few nm, and
- (ix) Are typically closely aligned with any Dauphiné twins.

Most of these quartz grains appear to have been exposed to temperatures high enough to partially melt the entire grain,

after which some portions remained amorphous while others recrystallized, sometimes as Dauphiné twins in alignment with the fractures. This evidence implies formation temperatures of >1713°C, quartz's melting point of quartz, and most likely at >2200°C, its boiling point. Multiple previous investigations have concluded that when amorphous silica is present within shock fractures or shock lamellae, its presence allows for the unequivocal differentiation between impact-related shock fractures and the glass-free lamellae that mark slow-strain tectonic deformation.

We conclude that glass-filled fractures support the hypothesis that a near-surface airburst occurred near the Abu Hureyra village. The shockwave from the low-altitude airburst coupled with the Earth's surface, thus producing extreme temperatures and pressures that fractured and melted quartz grains, melted or vaporized surficial sediments, and introduced molten silica into the fractures.

Acknowledgments

We are grateful to three reviewers whose thoughtful comments helped to improve the manuscript. We gratefully acknowledge the long-standing contributions of co-author Ted Bunch, a highly valued colleague and contributor who passed away while writing this manuscript. Dr. Bunch was one of the pioneers in identifying shocked quartz at Meteor Crater and elsewhere. We also appreciate the use of the CAMCOR facilities at the University of Oregon and the Electron Microscopy and Surface Analysis Laboratory at the University of Utah, along with assistance from EDAX, LLC. This work made use of the University of Utah USTAR shared facilities supported, in part, by the MRSEC Program of the NSF under Award #DMR-1121252. We also thank the thousands of donors and members of the Comet Research Group who have been crucial in making this research possible.

Author contributions

Conceptualization: A.M.T.M., J.P.K., M.L., M.C.R., Y-Q.L., G.K., S.M., W.S.W., A.W. Formal analysis: A.M.T.M., J.P.K., M.L., M.C.R., Y-Q.L., G.K., K.L., J.J.R., V.B., B.v.D., J.P.P., R.P., S.M., W.S.W., A.W. Investigation: A.M.T.M., J.P.K., M.L., M.C.R., Y-Q.L., G.K., K.L., J.J.R., V.B., B.v.D., J.P.P., R.P., S.M., W.S.W., A.W. Writing-original draft: A.M.T.M., J.P.K., M.L., M.C.R., Y-Q.L., G.K., S.M., W.S.W., A.W. Writing-review and editing: A.M.T.M., J.P.K., M.L., M.C.R., Y-Q.L., G.K., S.M., W.S.W., A.W. Funding acquisition: A.M.T.M., J.P.K., Y-Q.L., G.K., S.M., W.S.W., A.W.

Funding

Some funding was provided by the Czech Science Foundation (Grant 23-06075S). In particular, we thank Eugene Zhong,

who provided substantial gifts supporting this research to the University of South Carolina (C.R.M.) and the University of California, Santa Barbara (J.P.K). We also thank George Howard and the Cosmic Summit for contributions supporting this research.

Data availability statement

All essential data are published here. Multiple previous studies have completely expended the samples; hence, no more unprocessed sample material is available from the authors.

References

- [1] Moore, A.M.T.; Kennett, J.P.; Napier, W.M.; Bunch, T.E.; Weaver, J.C.; LeCompte, M.A.; Adedeji, A.V.; Kletetschka, G.; Hermes, R.E.; Wittke, J.H.; et al. Abu Hureyra, Syria, Part 2: Additional Evidence Supporting the Catastrophic Destruction of this Prehistoric Village by a Cosmic Airburst ~12,800 years ago. *ScienceOpen* **2023**, *1*, 1–36.
- [2] Moore, A.M.T.; Kennett, J.P.; Napier, W.M.; LeCompte, M.A.; Moore, C.R.; West, A. Abu Hureyra, Syria, Part 3: Comet Airbursts Triggered Major Climate Change 12,800 Years Ago that Initiated the Transition to Agriculture. *ScienceOpen* **2023**, *1*, 1–24.
- [3] Koeberl, C.; Reimold, W.U.; Cooper, G.; Cowan, D.; Vincent, P.M. Aourounga and Gwini Fada Impact Structures, Chad: Remote Sensing, Petrography, and Geochemistry of Target Rocks. *Meteorit. Planet. Sci.* **2005**, *40*, 1455–1471, doi:10.1111/j.1945-5100.2005.tb00412.x.
- [4] Kowitz, A.; Schmitt, R.T.; Uwe Reimold, W.; Hornemann, U. The First MEMIN Shock Recovery Experiments at Low Shock Pressure (5–12.5 GPa) with Dry, Porous Sandstone. *Meteorit. Planet. Sci.* **2013**, *48*, 99–114, doi:10.1111/maps.12030.
- [5] Reimold, W.U.; Crósta, A.P.; Hasch, M.; Kowitz, A.; Hauser, N.; Sanchez, J.P.; Simões, L.S.A.; de Oliveira, G.J.; Zaag, P.T. Shock Deformation Confirms the Impact Origin for the Cerro do Jarau, Rio Grande do Sul, Brazil, Structure. *Meteorit. Planet. Sci.* **2019**, *54*, 2384–2397, doi:10.1111/maps.13233.
- [6] Reimold, W.U.; Koeberl, C. Impact Structures in Africa: A Review. *J. Afr. Earth Sci.* **2014**, *93*, 57–175, doi:10.1016/j.jafrearsci.2014.01.008.
- [7] Gratz, A. Deformation in Laboratory-Shocked Quartz. *J. Non Cryst. Solids* **1984**, *67*, 543–558, doi:10.1016/0022-3093(84)90175-3.
- [8] Kowitz, A.; Güldemeister, N.; Schmitt, R.T.; Reimold, W.U.; Wünnemann, K.; Holzwarth, A. Revision and Recalibration of Existing Shock Classifications for Quartzose Rocks using Low-Shock Pressure (2.5–20 GPa) Recovery Experiments and Mesoscale Numerical Modeling. *Meteorit. Planet. Sci.* **2016**, *51*, 1741–1761, doi:10.1111/maps.12712.
- [9] Buchanan, P.; Reimold, W. Planar Deformation Features and Impact Glass in Inclusions from the Vredefort Granophyre, South Africa. *Meteorit. Planet. Sci.* **2002**, *37*, 807–822, doi:10.1111/j.1945-5100.2002.tb00857.x.
- [10] Hermes, R.E.; Wenk, H.-R.; Kennett, J.P.; Bunch, T.E.; Moore, C.R.; LeCompte, M.A.; Kletetschka, G.; Adedeji, A.V.; Langworthy, K.; Razink, J.; et al. Microstructures in Shocked Quartz: Linking Nuclear Airbursts and Meteorite Impacts. *Preprints* **2023**, 1–40. doi: 10.20944/preprints202308.0221.v1.
- [11] Goltrant, O.; Cordier, P.; Doukhan, J.-C. Planar Deformation Features in Shocked Quartz; a Transmission Electron Microscopy Investigation. *Earth Planet. Sci. Lett.* **1991**, *106*, 103–115, doi:10.1016/0012-821X(91)90066-Q.
- [12] Christie, J.; Ardell, A. Substructures of Deformation Lamellae in Quartz. *Geology* **1974**, *2*, 405–408, doi:10.1130/0091-7613(1974)2<405:SODLIQ>2.0.CO;2.
- [13] Bohor, B.; Fislser, D.; Gratz, A.J. Distinguishing between Shock and Tectonic Lamellae with the SEM. In *Proceedings of the Lunar and Planetary Science Conference*, 1995; pp. 145.
- [14] Gratz, A.J.; Fislser, D.K.; Bohor, B.F. Distinguishing Shocked from Tectonically Deformed Quartz by the use of the SEM and Chemical Etching. *Earth Planet. Sci. Lett.* **1996**, *142*, 513–521, doi:10.1016/0012-821X(96)00099-4.
- [15] Gratz, A.J.; Tyburczy, J.; Christie, J.; Ahrens, T.; Pongratz, P. Shock Metamorphism of Deformed Quartz. *Phys. Chem. Miner.* **1988**, *16*, 221–233, doi:10.1007/BF00220689.
- [16] Hamers, M.; Drury, M. Scanning Electron Microscope-Cathodoluminescence (SEM-CL) Imaging of Planar Deformation Features and Tectonic Deformation Lamellae in Quartz. *Meteorit. Planet. Sci.* **2011**, *46*, 1814–1831, doi:10.1111/j.1945-5100.2011.01295.x.
- [17] Stöffler, D.; Gault, D.; Wedekind, J.; Polkowski, G. Experimental Hypervelocity Impact into Quartz Sand: Distribution and Shock Metamorphism of Ejecta. *J. Geophys. Res.* **1975**, *80*, 4062–4077, doi:10.1029/JB080i029p04062.
- [18] Stöffler, D.; Langenhorst, F. Shock Metamorphism of Quartz in Nature and Experiment: I. Basic Observation and Theory. *Meteoritics* **1994**, *29*, 155–181, doi:10.1111/j.1945-5100.1994.tb00670.x.
- [19] Vernooij, M.G.; Langenhorst, F. Experimental Reproduction of Tectonic Deformation Lamellae in Quartz and Comparison to Shock-Induced Planar Deformation Features. *Meteorit. Planet. Sci.* **2005**, *40*, 1353–1361, doi:10.1111/j.1945-5100.2005.tb00406.x.
- [20] French, B.M.; Koeberl, C. The Convincing Identification of Terrestrial Meteorite Impact Structures: What Works, What Doesn't, and Why. *Earth Sci. Rev.* **2010**, *98*, 123–170, doi:10.1016/j.earscirev.2009.10.009.
- [21] Langenhorst, F. Shock Metamorphism of Some Minerals: Basic Introduction and Microstructural Observations. *Bull. Czech Geol. Surv.* **2002**, *77*, 265–282.
- [22] Ernstson, K.; Mayer, W.; Neumair, A.; Rappenglück, B.; Sudhaus, D. The Chiemgau Crater Strewn Field: Evidence of a Holocene Large Impact Event in Southeast Bavaria, Germany. *J. Sib. Fed.* **2010**, *3*, 72–103.
- [23] Ferriere, L.; Osinski, G.R. Shock Metamorphism. In *Impact Cratering: Processes and Products*; Osinski, G.R., Pierazzo, E., Eds.; John Wiley & Sons, 2012; pp. 106–124.
- [24] Christie, J.; Griggs, D.; Carter, N. Experimental Evidence of Basal Slip in Quartz. *J. Geol.* **1964**, *72*, 734–756, doi:10.1086/627030.
- [25] Christie, J.M.; Raleigh, C.B. The Origin of Deformation Lamellae in Quartz. *Am. J. Sci.* **1959**, *257*, 385–407, doi:10.2475/ajs.257.6.385.

- [26] McLaren, A.; Retchford, J.; Griggs, D.; Christie, J. Transmission Electron Microscope Study of Brazil Twins and Dislocations Experimentally Produced in Natural Quartz. *Phys. Status Solidi (B)* **1967**, *19*, 631–644, doi:10.1002/pssb.19670190216.
- [27] McLaren, A.; Turner, R.; Boland, J.; Hobbs, B. Dislocation Structure of the Deformation Lamellae in Synthetic Quartz; a Study by Electron and Optical Microscopy. *Contrib. Mineral. Petrol.* **1970**, *29*, 104–115, doi:10.1007/BF00392018.
- [28] Kieffer, S.W. Shock Metamorphism of the Coconino Sandstone at Meteor Crater, Arizona. *J. Geophys. Res.* **1971**, *76*, 5449–5473, doi:10.1029/JB076i023p05449.
- [29] Kieffer, S.W.; Phahey, P.P.; Christie, J.M. Shock Processes in Porous Quartzite: Transmission Electron Microscope Observations and Theory. *Contrib. Mineral. Petrol.* **1976**, *59*, 41–93, doi:10.1007/BF00375110.
- [30] Ernstson, K. Evidence of Meteorite Impact-Induced Thermal Shock in Quartz. In *Proceedings of the Modern Problems of Theoretical, Experimental, and Applied Mineralogy*, Syktyvkar, Russia, 2020; pp. 1423, doi:10.19110/98491-014-361-362.
- [31] Ernstson, K.; Bauer, F.; Hiltl, M. A Prominent Iron Silicides Strewn Field and Its Relation to the Bronze Age/Iron Age Chiemgau Meteorite Impact Event (Germany). *Earth Sci.* **2023**, *12*, 26–40, doi:10.11648/j.earth.20231201.14.
- [32] Ernstson, K.; Sideris, C.; Liritzis, I.; Neumair, A. The Chiemgau Meteorite Impact Signature of the Stötham Archaeological Site (Southeast Germany). *Mediterr. Archaeol. Archaeom.* **2012**, *12*, 249–259.
- [33] Ernstson, K. Meteorite Impact spAllation: From Mega- to Micro-Scale. Available online: <http://www.impact-structures.com/impact-educational/meteorite-impact-spallation-from-mega-to-micro-scale/> (accessed on 3 May 2023).
- [34] Kowitz, A.; Güldemeister, N.; Reimold, W.; Schmitt, R.; Wünnemann, K. Diaplectic Quartz Glass and SiO₂ Melt Experimentally Generated at Only 5 GPa Shock Pressure in Porous Sandstone: Laboratory Observations and Meso-Scale Numerical Modeling. *Earth Planet. Sci. Lett.* **2013**, *384*, 17–26, doi:10.1016/j.epsl.2013.09.021.
- [35] Bunch, T.E.; Hermes, R.E.; Moore, A.M.; Kennett, D.J.; Weaver, J.C.; Wittke, J.H.; DeCarli, P.S.; Bischoff, J.L.; Hillman, G.C.; Howard, G.A. Very High-Temperature Impact Melt Products as Evidence for Cosmic Airbursts and Impacts 12,900 Years Ago. *Proc. Natl. Acad. Sci. USA* **2012**, *109*, E1903–E1912, doi:10.1073/pnas.1204453109.
- [36] Moore, A.; Kennett, D. Cosmic Impact, the Younger Dryas, Abu Hureyra, and the Inception of Agriculture in Western Asia. *Eurasian Prehist* **2013**, *10*, 57–66.
- [37] Moore, A.M.T.; Kennett, J.P.; Napier, W.M.; Bunch, T.E.; Weaver, J.C.; LeCompte, M.; Adedji, V.; Hackley, P.; Kletetschka, G.K.; Hermes, R.E.; et al. Evidence of Cosmic Impact at Abu Hureyra, Syria at the Younger Dryas Onset (~12.8 ka): High-Temperature Melting at >2200°C. *Sci. Rep.* **2020**, *10*, 4185, doi:10.1038/s41598-020-60867-w.
- [38] Moore, A.; Hillman, G.; Legge, A. *Village on the Euphrates: From Foraging to Farming at Abu Hureyra*; Oxford University Press: London, New York, 2000.
- [39] Smith, A.; Oechsner, A.; Rowley-Conwy, P.; Moore, A.M. Epipalaeolithic Animal Tending to Neolithic Herding at Abu Hureyra, Syria (12,800–7,800 calBP): Deciphering Dung Spherulites. *PLoS One* **2022**, *17*, e0272947, doi:10.1371/journal.pone.0272947.
- [40] Firestone, R.B.; West, A.; Kennett, J.; Becker, L.; Bunch, T.; Revay, Z.; Schultz, P.; Belgya, T.; Kennett, D.; Erlandson, J. Evidence for an Extraterrestrial Impact 12,900 Years Ago that Contributed to the Megafaunal Extinctions and the Younger Dryas Cooling. *Proc. Natl. Acad. Sci. USA* **2007**, *104*, 16016–16021, doi:10.1073/pnas.0706977104.
- [41] Fayek, M.; Anovitz, L.M.; Allard, L.F.; Hull, S. Framboidal Iron Oxide: Chondrite-Like Material from the Black Mat, Murray Springs, Arizona. *Earth Planet. Sci. Lett.* **2012**, *319*, 251–258, doi:10.1016/j.epsl.2011.11.033.
- [42] Israde-Alcántara, I.; Bischoff, J.L.; Domínguez-Vázquez, G.; Li, H.-C.; DeCarli, P.S.; Bunch, T.E.; Wittke, J.H.; Weaver, J.C.; Firestone, R.B.; West, A. Evidence from Central Mexico Supporting the Younger Dryas Extraterrestrial Impact Hypothesis. *Proc. Natl. Acad. Sci. USA* **2012**, *109*, E738–E747, doi:10.1073/pnas.1110614109.
- [43] LeCompte, M.A.; Goodyear, A.C.; Demitroff, M.N.; Batchelor, D.; Vogel, E.K.; Mooney, C.; Rock, B.N.; Seidel, A.W. Independent Evaluation of Conflicting Microspherule Results from Different Investigations of the Younger Dryas Impact Hypothesis. *Proc. Natl. Acad. Sci. USA* **2012**, *109*, E2960–E2969, doi:10.1073/pnas.1208603109.
- [44] Wittke, J.H.; Weaver, J.C.; Bunch, T.E.; Kennett, J.P.; Kennett, D.J.; Moore, A.M.T.; Hillman, G.C.; Tankersley, K.B.; Goodyear, A.C.; Moore, C.R.; et al. Evidence for Deposition of 10 Million Tonnes of Impact Spherules Across Four Continents 12,800 y Ago. *Proc. Natl. Acad. Sci. USA* **2013**, *110*, E2088–E2097, doi:10.1073/pnas.1301760110.
- [45] Moore, C.R.; West, A.; LeCompte, M.A.; Brooks, M.J.; Daniel Jr, I.R.; Goodyear, A.C.; Ferguson, T.A.; Ivester, A.H.; Feathers, J.K.; Kennett, J.P.; et al. Widespread Platinum Anomaly Documented at the Younger Dryas Onset in North American Sedimentary Sequences. *Sci. Rep.* **2017**, *7*, 44031, doi:10.1038/srep44031.
- [46] Mahaney, W.C. Evidence from the Northwestern Venezuelan Andes for Extraterrestrial Impact: The Black Mat Enigma. *Geomorphology* **2010**, *116*, 48–57, doi:10.1016/j.geomorph.2009.10.007.
- [47] Mahaney, W.C. Cosmic Airburst on Developing Allerød Substrates (Soils) in the Western Alps, Mt. Viso Area. *Stud. Quat.* **2018**, *35*, 1–21, doi:10.2478/squa-2018-0001.
- [48] Kennett, J.; Kennett, D.; LeCompte, M.; West, A. Potential Consequences of the YDB Cosmic Impact at 12.8 ka. In *Early Human Life on the Southeastern Coastal Plain*; Goodyear, A.C., Moore, A.M., Eds.; University Press of Florida: Gainesville, FL, 2018; pp. 175–192.
- [49] Kennett, J.P.; Kennett, D.J.; Culleton, B.J.; Aura Tortosa, J.E.; Bischoff, J.L.; Bunch, T.E.; Daniel, I.R.; Erlandson, J.M.; Ferraro, D.; Firestone, R.B.; et al. Bayesian Chronological Analyses Consistent with Synchronous Age of 12,835–12,735 Cal B.P. for Younger Dryas Boundary on Four Continents. *Proc. Natl. Acad. Sci. USA* **2015**, *112*, E4344–E4353, doi:10.1073/pnas.1507146112.
- [50] Kennett, D.J.; Kennett, J.P.; West, A.; Mercer, C.; Hee, S.S.Q.; Bement, L.; Bunch, T.E.; Sellers, M.; Wobach, W.S. Nanodiamonds in the Younger Dryas Boundary Sediment Layer. *Science* **2009**, *323*, 94, doi:10.1126/science.1162819.
- [51] Wobach, W.S.; Ballard, J.P.; Mayewski, P.A.; Adedji, V.; Bunch, T.E.; Firestone, R.B.; French, T.A.; Howard, G.A.; Israde-Alcántara, I.; Johnson, J.R. Extraordinary Biomass-Burning Episode and Impact Winter Triggered by the Younger Dryas Cosmic Impact ~12,800 Years Ago. 1. Ice Cores and Glaciers. *J. Geol.* **2018**, *126*, 165–184, doi:10.1086/695703.
- [52] Wobach, W.S.; Ballard, J.P.; Mayewski, P.A.; Parnell, A.C.; Cahill, N.; Adedji, V.; Bunch, T.E.; Domínguez-Vázquez, G.; Erlandson, J.M.; Firestone, R.B. Extraordinary Biomass-Burning Episode and Impact Winter Triggered by the Younger Dryas Cosmic Impact ~12,800 Years Ago. 2. Lake, Marine, and Terrestrial Sediments. *J. Geol.* **2018**, *126*, 185–205, doi:10.1086/695704.
- [53] LeCompte, M.A.; West, A.; Adedji, A.; Demitroff, M.; Witwer, T.; Langenburg, R.A. The Bowser Road Mastodon and the Younger Dryas Impact Hypothesis, Appendix 3. In *The Archaeological Recovery of the Bowser Road Mastodon, Orange County NY*; Gramly, R., Ed.; Persimmon Press: Santa Clara, CA, 2017.
- [54] Pino, M.; Abarzúa, A.M.; Astorga, G.; Martel-Cea, A.; Cossio-Montecinos, N.; Navarro, R.X.; Lira, M.P.; Labarca, R.; LeCompte, M.A.; Adedji, V.; et al. Sedimentary Record from Patagonia, Southern Chile Supports Cosmic-Impact Triggering of Biomass

- Burning, Climate Change, and Megafaunal Extinctions at 12.8 ka. *Sci. Rep.* **2019**, 9, 4413, doi:10.1038/s41598-018-38089-y.
- [55] Teller, J.; Boyd, M.; LeCompte, M.; Kennett, J.; West, A.; Telka, A.; Diaz, A.; Adedeji, V.; Batchelor, D.; Mooney, C. A Multi-Proxy Study of Changing Environmental Conditions in a Younger Dryas Sequence in Southwestern Manitoba, Canada, and Evidence for an Extraterrestrial Event. *Quat. Res.* **2019**, 93, 60–87, doi:10.1017/qua.2019.46.
- [56] Wu, Y.; Sharma, M.; LeCompte, M.A.; Demitroff, M.N.; Landis, J.D. Origin and Provenance of Spherules and Magnetic Grains at the Younger Dryas Boundary. *Proc. Natl. Acad. Sci. USA* **2013**, 110, E3557–E3566, doi:10.1073/pnas.1304059110.
- [57] Thackeray, J.F.; Scott, L. The Younger Dryas in the Wonderkrater Sequence, South Africa? *Ann. Transvaal Mus.* **2006**, 43, 111–112.
- [58] Kinzie, C.R.; Que Hee, S.S.; Stich, A.; Tague, K.A.; Mercer, C.; Razink, J.J.; Kennett, D.J.; DeCarli, P.S.; Bunch, T.E.; Wittke, J.H. Nanodiamond-Rich Layer Across Three Continents Consistent with Major Cosmic Impact at 12,800 cal BP. *J. Geol.* **2014**, 122, 475–506, doi:10.1086/677046.
- [59] Petaev, M.I.; Huang, S.; Jacobsen, S.B.; Zindler, A. Large Pt Anomaly in the Greenland Ice Core Points to a Cataclysm at the Onset of Younger Dryas. *Proc. Natl. Acad. Sci. USA* **2013**, 110, 12917–12920, doi:10.1073/pnas.1303924110.
- [60] Andronikov, A.; Lauretta, D.; Andronikova, I.; Maxwell, R. On the Possibility of a Late Pleistocene Extraterrestrial Impact: LA-ICP-MS Analysis of the Black Mat and Usselo Horizon Samples. In *Proceedings of the 74th Annual Meteoritical Society Meeting*, London, 2011; pp. A11, doi:10.1111/j.1945-5100.2011.01221.x.
- [61] Andronikov, A.; Subetto, D.; Lauretta, D.; Andronikova, I.; Drosenko, D.; Kuznetsov, D.; Sapelko, T.; Syrykh, L. In Search for Fingerprints of an Extraterrestrial Event: Trace Element Characteristics of Sediments from the Lake Medvedevskoye (Karelian Isthmus, Russia). *Dokl. Earth Sci.* **2014**, 457, 819–823, doi:10.1134/S1028334X14070022.
- [62] Andronikov, A.V.; Andronikova, I.E. Sediments from Around the Lower Younger Dryas Boundary (USA): Implications from LA-ICP-Analysis. *Geogr. Ann. A* **2016**, 98, 221–236, doi:10.1111/geoa.12132.
- [63] Andronikov, A.V.; Andronikova, I.E.; Loehn, C.W.; Lafuente, B.; Ballenger, J.A.; Crawford, G.T.; Lauretta, D.S. Implications from Chemical, Structural and Mineralogical Studies of Magnetic Microspherules from Around the Lower Younger Dryas Boundary (New Mexico, USA). *Geogr. Ann. A* **2016**, 98, 39–59, doi:10.1111/geoa.12122.
- [64] Andronikov, A.V.; Rudnickaitė, E.; Lauretta, D.S.; Andronikova, I.E.; Kaminskas, D.; Šinkūnas, P.; Melešytė, M. Geochemical Evidence of the Presence of Volcanic and Meteoritic Materials in Late Pleistocene Lake Sediments of Lithuania. *Quat. Int.* **2015**, 386, 18–29, doi:10.1016/j.quaint.2014.10.005.
- [65] Boslough, M. Computational Modeling of Low-Altitude Airbursts. In *Proceedings of the AGU Fall Meeting Abstracts, #U21E-03*, San Francisco, CA, 2007.
- [66] Boslough, M. Airburst Modeling. In *Proceedings of the First International Workshop on Potentially Hazardous Asteroids Characterization, Atmospheric Entry and Risk Assessment*, NASA Ames Research Center, Mountain View, CA, 2015.
- [67] Boslough, M.; Crawford, D.A. Low-Altitude Airbursts and the Impact Threat. *Int. J. Impact. Eng.* **2008**, 35, 1441–1448, doi:10.1016/j.ijimpeng.2008.07.053.
- [68] Demitroff, M.; LeCompte, M.; Rock, B. Cold Climate Related Structural Sinks Accommodate Unusual Soil Constituents, Pinelands National Reserve, New Jersey, USA. In *Proceedings of the AGU Fall Meeting Abstracts*, 2009; pp. PP31D-1394.
- [69] Ballard, J.P.; Bijkerk, A.K. Quartz Melt Structures in European Coversands May Support Younger Dryas Extraterrestrial Impact Hypothesis. In *Proceedings of the UT Geography Research Symposium 2014 “Mapping Outside the Lines: Geography as a Nexus for Interdisciplinary and Collaborative Research”*, Knoxville, Tennessee, 2014.
- [70] Van Hoesel, A.; Hoek, W.Z.; Pennock, G.M.; Kaiser, K.; Plümper, O.; Jankowski, M.; Hamers, M.F.; Schlaak, N.; Küster, M.; Andronikov, A.V. A Search for Shocked Quartz Grains in the Allerød-Younger Dryas Boundary Layer. *Meteorit. Planet. Sci.* **2015**, 50, 483–498, doi:10.1111/maps.12435.
- [71] Blenkinsop, T. Shock-Induced Microstructures and Shock Metamorphism. In *Deformation Microstructures and Mechanisms in Minerals and Rocks*; 2000; pp. 80–89, doi:10.1007/0-306-47543-X.
- [72] Bohor, B.; Betterton, W.; Krogh, T. Impact-Shocked Zircons: Discovery of Shock-Induced Textures Reflecting Increasing Degrees of Shock Metamorphism. *Earth Planet. Sci. Lett.* **1993**, 119, 419–424, doi:10.1016/0012-821X(93)90149-4.
- [73] Hamers, M.; Pennock, G.; Drury, M. Scanning Electron Microscope Cathodoluminescence Imaging of Subgrain Boundaries, Twins and Planar Deformation Features in Quartz. *Phys. Chem. Mineral.* **2017**, 44, 263–275, doi:10.1007/s00269-016-0858-x.
- [74] Hamers, M.F. *Identifying Shock Microstructures in Quartz from Terrestrial Impacts: New Scanning Electron Microscopy Methods*; UU Department of Earth Sciences, 2013.
- [75] Hamers, M.F.; Pennock, G.M.; Herwegh, M.; Drury, M.R. Distinction between Amorphous and Healed Planar Deformation Features in Shocked Quartz using Composite Color Scanning Electron Microscope Cathodoluminescence (SEM-CL) Imaging. *Meteorit. Planet. Sci.* **2016**, 51, 1914–1931, doi:10.1111/maps.12711.
- [76] Kalceff, M.A.S.; Phillips, M.R.; Moon, A.R.; Kalceff, W. Cathodoluminescence Microcharacterisation of Silicon Dioxide Polymorphs. In *Cathodoluminescence in Geosciences*; Springer, 2000; pp. 193–224.
- [77] Madden, M.E.E.; Kring, D.A.; Bodnar, R.J. Shock Re-equilibration of Fluid Inclusions in Coconino Sandstone from Meteor Crater, Arizona. *Earth Planet. Sci. Lett.* **2006**, 241, 32–46.
- [78] Langenhorst, F. Shock Experiments on Pre-Heated α - and β -Quartz: II. X-Ray and TEM Investigations. *Earth Planet. Sci. Lett.* **1994**, 128, 683–698, doi:10.1016/0012-821X(94)90179-1.
- [79] Gleason, A.; Bolme, C.; Lee, H.; Nagler, B.; Galtier, E.; Kraus, R.; Sandberg, R.; Yang, W.; Langenhorst, F.; Mao, W. Time-Resolved Diffraction of Shock-Released SiO₂ and Diaplectic Glass Formation. *Nat. Commun.* **2017**, 8, 1–6, doi:10.1038/s41467-017-01791-y.
- [80] Schubnikow, A.; Zinserling, K. Über die Schlag- und Druckfiguren und über die mechanischen Quarzzwillinge. *Z. für Krist. Cryst. Mater.* **1932**, 83, 243–264, doi:10.1524/zkri.1932.83.1.243.
- [81] Wenk, H.-R.; Janssen, C.; Kenkmann, T.; Dresen, G. Mechanical Twinning in Quartz: Shock Experiments, Impact, Pseudotachylites and Fault Breccias. *Tectonophysics* **2011**, 510, 69–79, doi:10.1016/j.tecto.2011.06.016.
- [82] Wenk, H.-R.; Lonardelli, I.; Vogel, S.; Tullis, J. Dauphiné Twinning as Evidence for an Impact Origin of Preferred Orientation in Quartzite: An Example from Vredefort, South Africa. *Geology* **2005**, 33, 273–276, doi:10.1130/G21163.1.
- [83] Osinski, G.R.; Kieniewicz, J.; Smith, J.R.; Boslough, M.; Eccleston, M.; Schwarcz, H.P.; Kleindienst, M.R.; Haldemann, A.F.C.; Churcher, C.S. The Dakhleh Glass: Product of an Impact Airburst or Cratering Event in the Western Desert of Egypt? *Meteorit. Planet. Sci.* **2008**, 43, 2089–2106, doi:10.1111/j.1945-5100.2008.tb00663.x.
- [84] Schultz, P.H.; Harris, R.S.; Perroud, S.; Blanco, N.; Tomlinson, A.J. Widespread Glasses Generated by Cometary Fireballs during the Late Pleistocene in the Atacama Desert, Chile. *Geology* **2022**, 50, 205–209, doi:10.1130/G49426.1.
- [85] Kenkmann, T.; Hornemann, U.; Stöffler, D. Experimental Generation of Shock-Induced Pseudotachylites Along Lithological Interfaces. *Meteorit. Planet. Sci.* **2000**, 35, 1275–1290, doi:10.1111/j.1945-5100.2000.tb01516.x.

- [86] Stöffler, D. Glasses Formed by Hypervelocity Impact. *J. Non Cryst. Solids* **1984**, 67, 465–502, doi:10.1016/0022-3093(84)90171-6.
- [87] Stöffler, D.; Grieve, R. *Metamorphic Rocks: A Classification and Glossary of Terms, Recommendation of the International Union of Geological Sciences*; 2007.
- [88] Fazio, A.; Pollok, K.; Langenhorst, F. Experimental Evidence for Mechanical Brazil Twins as an Indicator of Low-Pressure Shock Metamorphism (<17.5 GPa). *Geology* **2018**, 46, 787–790, doi:10.1130/G40198.1.
- [89] Wilk, J.; Hamann, C.; Fazio, A.; Luther, R.; Hecht, L.; Langenhorst, F.; Kenkmann, T. Petrographic Investigation of Shatter Cone Melt Films Recovered from MEMIN Impact Experiments in Sandstone and iSALE Modeling of their Formation Boundary Conditions. *Meteorit. Planet. Sci.* **2018**, 53, 1569–1593, doi:10.1111/maps.13179.
- [90] Martinelli, G.; Plescia, P.; Tempesta, E.; Paris, E.; Gallucci, F. Fracture Analysis of α -Quartz Crystals Subjected to Shear Stress. *Minerals* **2020**, 10, 870, doi:10.3390/min10100870.
- [91] Ernstson, K.; Müller, W.; Gawlik-Wagner, A. The Saarlouis Semi Crater Structure: Notable Insight into the Saarland (Germany) Meteorite Impact Event Achieved, Abstract and Poster #1876. In *Proceedings of the 49th Lunar and Planetary Science Conference*, 2018, doi:10.13140/RG.2.2.20958.74560.
- [92] Eckert, J.; Gourdon, O.; Jacob, D.E.; Meral, C.; Monteiro, P.J.; Vogel, S.C.; Wirth, R.; Wenk, H.-R. Ordering of Water in Opals with Different Microstructures. *Eur. J. Mineral.* **2015**, 27, 203–213, doi:10.1127/ejm/2015/0027-2428.
- [93] Wenk, H.-R.; Chandler, B.C.; Chen, K.; Li, Y.; Tamura, N.; Yu, R. Residual Lattice Strain in Quartzites as a Potential Palaeo-Piezometer. *Geophys. J. Int.* **2020**, 222, 1363–1378, doi:10.1093/gji/ggaa226.
- [94] Wenk, H.-R.; Yu, R.; Vogel, S.; Vasin, R. Preferred Orientation of Quartz in Metamorphic Rocks from the Bergell Alps. *Minerals* **2019**, 9, 277, doi:10.3390/min9050277.
- [95] Barber, D.; Wenk, H.-R. Dauphiné Twinning in Deformed Quartzites: Implications of an In Situ TEM Study of the α - β Phase Transformation. *Phys. Chem. Mineral.* **1991**, 17, 492–502, doi:10.1007/BF00202229.
- [96] Ernstson, K. Looking into the Cobbles. Available online: <http://www.impact-structures.com/impact-spain/shock-deformation-in-triassic-buntsandstein-conglomerates-spain/looking-into-the-cobbles/> (accessed on January 2023).
- [97] Ernstson, K. The Subparallel Fracturing. Available online: <http://www.impact-structures.com/impact-spain/shock-deformation-in-triassic-buntsandstein-conglomerates-spain/the-subparallel-fracturing/> (accessed on January 2023).
- [98] Bunch, T.E.; LeCompte, M.A.; Adedeji, A.V.; Wittke, J.H.; Burleigh, T.D.; Hermes, R.E.; Mooney, C.; Batchelor, D.; Wolbach, W.S.; Kathan, J.; et al. A Tunguska Sized Airburst Destroyed Tall el-Hammam a Middle Bronze Age City in the Jordan Valley Near the Dead Sea. *Sci. Rep.* **2021**, 11, 1–64, doi:10.1038/s41598-021-97778-3.

Appendix, methods: Instrumentation and analytical details

Candidate grains were investigated using a robust series of analyses using a wide range of high-resolution instruments as follows and adapted from Hermes et al. [10]. These included optical transmission microscopy (OPT), epi-illumination microscopy (EPI), scanning electron microscopy (SEM), energy dispersive spectroscopy (EDS), focused ion beam milling (FIB), transmission electron microscopy (TEM), scanning transmission electron microscopy (STEM), fast-Fourier transform (FFT), electron backscatter diffraction (EBSD), cathodoluminescence (CL), and micro-Raman.

Thin-sectioned slides

Selected sedimentary grains were wet-sieved to concentrate those between diameters of ~150 (#100 ASTM sieve) to ~850 μm (#20 ASTM sieve). Then, the sorted grains were treated with HCl to destroy carbonates. Grains were embedded in blue epoxy for better visibility, covering the entire 27 \times 46 mm slide, and were sectioned at Spectrum Petrographics, Vancouver, WA. Sectioned slides were given a high-polish, microprobe-grade finish necessary for EBSD analyses. No cover slide was used.

Hf etching

Following Bunch et al. [98], Spectrum Petrographics, Vancouver, WA, etched thin-sectioned slides by exposure to 50% HF vapor for 2 min to dissolve amorphous quartz and make any lamellae more visible. Note that exposure for <2 min was insufficient for etching and exposing shock

fractures; exposure for >2 min can damage the slides. After treatment with HF vapor, we performed another dH_2O rinse.

Alternately, we treated some slides with liquid HF for 2 min, after which we performed a dH_2O rinse; neutralized them with 5% sodium carbonate solution; rinsed them with dH_2O again; then treated them with 5% HCl to remove carbonates. The HF vapor produced more consistent results than the liquid HF.

Multiple studies [7, 13, 14, 16, 71, 72] have demonstrated the utility of etching quartz grains with HF to differentiate between glass-filled shock features and glass-free tectonic deformation lamellae. In our study, we observed that HF sometimes lightly etches tectonic deformation lamellae to reveal broad, shallow depressions, as others reported [13, 71]. However, unlike shock fractures, these depressions in the damaged lattice did not extend more than a few microns into the grain and were not observed to contain amorphous silica.

Optical transmission microscopy (OPT)

For this study, we made polished thin sections of quartz grains and meltglass to search for potentially shocked quartz grains. Grains were examined using a petrographic polarizing microscope with a rotary stage. The microscope was equipped with transmitted light and epi-illumination (reflected light). First, epi-illumination and transmitted light were used with objective lenses ranging from 04 \times to 100 \times magnification. Once a candidate grain was identified, it was rotated to extinction under cross polars. Photomicrographs were acquired under both transmitted light and epi-illumination.

Epi-illumination microscopy (EPI)

This optical technique uses reflected light to image the surfaces of the grains investigated.

Scanning electron microscopy (SEM)

Standard practices were used for SEM analyses. At the University of Oregon, we used a ThermoFisher Apreo 2 SEM with a CL detector. At Elizabeth City State University, North Carolina, SEM images were acquired in low-vacuum mode using a JEOL-6000 SEM system.

Energy dispersive spectroscopy (EDS)

SEM- and TEM-based EDS exposes a specimen to an electron beam that generates X-rays that vary according to the elements present in the sample. Standard practices were used for TEM analyses.

Using SEM-EDS, we manually selected for detection of major elements with uncertainties of approximately $\pm 10\%$. At the University of Utah, secondary and backscattered electron images were collected using a Teneo SEM system (Thermofisher FEI, Hillsboro, OR).

Focused ion beam milling (FIB)

This is a technique to prepare a thin specimen (avg: ~ 175 nanometers (nm) thick) by milling a quartz grain with focused gallium (Ga) ions. The resulting specimen, called a foil, is then analyzed using TEM.

At the CAMCOR facility of the University of Oregon, TEM samples of quartz foils were prepared using a Helios Dual Beam SEM FIB. At the Surface Analysis Laboratory at the University of Utah, TEM sample preparation of quartz foils from bulk specimens was performed on an FEI/Thermo Helios Nanolab 650. The lift-out procedure followed standard sample preparation techniques. First, an electron beam deposited a platinum layer locally. Next, an ion beam was used to deposit an additional platinum layer. Trenches were milled on each side of the protective layer. Cuts were then made to the underside, and a micromanipulator probe was placed in contact with the surface (Omniprobe 200). The probe was attached by depositing platinum, and the sample was cut free from the bulk. The lift-out was attached to a copper support grid using the micromanipulator probe. The sample was then thinned using the ion beam at progressively decreasing accelerating voltages, 30 kV, 16 kV, 8 kV, and 2 kV.

Transmission electron microscopy (TEM)

TEM images were also acquired on the FIB foils. Standard practices were used for TEM analyses.

Selected area diffraction (SAD)

When an electron beam passes through a thin FIB foil of quartz, the electron beam's interaction with the quartz atoms creates an electron diffraction pattern. SAD can reveal details of the grain's lattice parameters and crystalline orientation or the lack of structure in amorphous silica.

Scanning transmission electron microscopy (STEM)

Bright-field STEM images were acquired on focused ion beam foils. Standard practices were used for STEM analyses.

At the CAMCOR facility at the University of Oregon, Transmission/Scanning transmission electron microscopy, or (S)TEM, was performed on an FEI 80-300 Titan scanning/transmission electron microscope (STEM) equipped with an image corrector, High-Angle Annular Dark Field (HAADF) detector, Energy Dispersive X-ray Spectroscopy (EDS) detector, Gatan Imaging Filter (GIF), and a 4-megapixel Charge-Coupled Device (CCD) camera. Microscope magnification was calibrated using a standard cross-grating carbon replica (2,160 lines/mm) evaporated with Au-Pd (Ted Pella #607). All images, diffraction patterns, and EDX maps were collected at 300 Kv and processed using Digital Micrograph, version 3.32.2403.0. Because electron microscopy is capable of causing irradiation-induced amorphization [18], quartz grains were examined at low magnification using low voltages and very short image-acquisition times. We confirmed that we were not creating amorphous quartz by viewing the nearby crystalline lattice.

At the University of Utah, STEM/TEM was performed on a JEOL 2800 operated at 200 kV. EDS data was collected and processed using ThermoFisher Noran System 7 software. Spectral maps were processed as net counts (background subtracted) using a 5×5 kernel size. Quantitative results were obtained using the Cliff-Lorimer method with absorption correction.

Fast-Fourier transform (FFT) and inverse Fast-Fourier transform (IFFT)

The diffraction characteristics of the FIB foils were investigated using FFT, an image processing technique for analyzing high-resolution TEM (HRTEM) images in reciprocal space. The FFT algorithm calculates the frequency distribution of pixel intensities in an HRTEM image and then displays any periodicity as spots in an output image, thus revealing the crystal's structure. HRTEM and FFT allow the measurement of interatomic spacings, known as d-spacings, measured in nm or angstroms (\AA). IFFT imagery is derived from spot diffraction patterns in an FFT image and is used to show the areas of the crystalline structure that contribute to the diffraction spots shown in an FFT image.

Cathodoluminescence (SEM-CL)

Luminescence occurs in the SEM when high-energy electrons bombard some materials. After that, photons are emitted at characteristic wavelengths, and those emissions are recorded in panchromatic (185–850 nm wavelengths) and 3-filtered (RGB) formats. Red, green, and blue channels were optimized individually to obtain the maximum information from the image. Thus, the color information in the images is non-quantitative. They were composited to create a 24-bit color image.

At the University of Oregon, we used a ThermoFisher Apreo 2 SEM with a CL detector. The cathodoluminescent (CL) images were synchronously captured at red (R), green (G), and blue (B) wavelengths on coated thin sections in low-vacuum mode on a Thermo Apreo2 S FE-SEM at 10 kV using 3.2 nA of beam current at ~10 mm working distance with 50 Pa of chamber pressure to balance charge. Wavelength ranges: red: 595–813 nm; green: 495–615; and blue: 291–509 nm. Backscatter (BSE) and secondary (SE) electron images were captured with similar beam settings.

Micro-Raman

We investigated the shock fractures using micro-Raman. The objective magnification is 100×, and the laser power is 20 mW at 780 nm with an integration time of 5 s. By mounting the thin-sectioned slide on a motorized stage and collecting Raman spectra at specified intervals, it is possible to analyze the spectra and determine whether areas contain crystalline quartz and amorphous silica.

Electron backscatter diffraction (EBSD)

This is an SEM-based analytical technique in which an electron beam scans across a crystalline sample tilted at 70°. The diffracted electrons produce what are called Kikuchi patterns that reveal the microstructural properties of the sample. EBSD was also used to determine the quartz grains' crystallographic orientations. We often used an EBSD technique called "PRIAS," an acronym for "Pattern Region of Interest Analysis System."

At the University of Utah, secondary and backscattered electron SEM images were collected using a Teneo system (ThermoFisher FEI; Hillsboro, OR). EDS, EBSD, and CL

analyses were similarly conducted with the same SEM system installed with the following detectors: an Octane Elite EDS system (EDAX, Pleasanton, CA) was used to collect elemental spectra; a Monarc CL Detector (Gatan; Pleasanton, CA) was used for cathodoluminescence studies. SEM beam energy and current were optimized to meet the requirements of each analysis mode. Before imaging, sample slides were polished to 0.20 μm roughness with colloidal silica suspension and washed with water to remove residues. The slides were then coated with 5-nm-thick carbon using a Leica EM ACE600 coater (Leica Microsystems, Inc., Deerfield, IL) to prevent charging during the imaging process.

Universal stage

We also investigated the shock fractures using the universal stage. However, we could not determine Miller indices because the observed shock fractures are non-planar and not oriented along the quartz crystals' crystallographic planes and, thus, cannot be accurately measured and compared to planar features.

Image processing

Most images were globally adjusted for balance, brightness, contrast, and sharpness, and some images were cropped to fit the space. A few images were rotated for clarity, and the legends and scale bars were repositioned at the bottom of the figures. Legends sometimes became unreadable for RGB images and some resized images, so they were replaced with the original legend. EDS figures were composited from multiple channels. No data within the figures were changed or obscured in making any adjustments.